ANALYSIS AND SIMULATION
OF A VIRTUAL PISTON PUMP

by

Nassib S. Aouad

Submitted in Partial Fulfillment of the Requirements

for the Degree of

Masters of Science

in the

Mechanical Engineering

Program

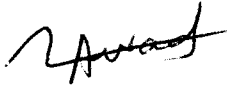YOUNGSTOWN STATE UNIVERSITY

August, 2004

ANALYSIS AND SIMULATION
OF A VIRTUAL PISTON PUMP

by

Nassib S. Aouad

I hereby release this thesis to the public. I understand this thesis will be made available from the OhioLINK ETD Center and the Maag Library Circulation Desk for public access. I also authorize the University or other individuals to make copies of this thesis as needed for scholarly research.
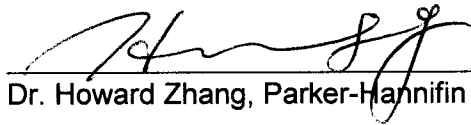
Signature:

_____ 8/6/04
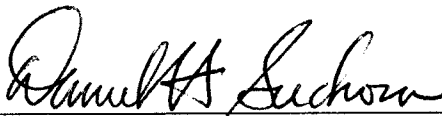Nassib S. Aouad, Student   Date

Approvals:

_____ 8/6/04
Dr. Ganesh Kudav, Professor at YSU-Thesis Advisor   Date

_____ 8/11/04
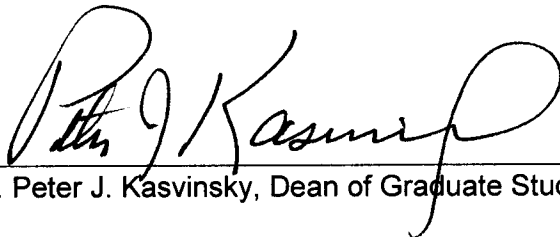Dr. Howard Zhang, Parker-Hannifin Corp.-Committee Member   Date

_____ 8/6/04
Dr. Daniel Suchora, Professor at YSU-Committee Member   Date

_____ 8/6/04
Dr. Peter J. Kasvinsky, Dean of Graduate Studies   Date

LIST OF FIGURES

LIST OF TABLES

LIST OF SYMBOLS

P: The pressure on the piston at the instant considered

A_p: The piston area

R: The piston pitch radius

a: The distance from the piston-slipper joint axis to the swash plate pivot

α: The swash plate angle

e: The eccentricity of the swash plate pivot with respect to barrel pivot

u: The linear deformations of the nodes of the finite element mode

Φ: The shape vectors or mode shapes

q: The vector of modal coordinates

$\hat{K}$: The generalized stiffness matrix

$\hat{M}$: The generalized mass matrix

Φ^*_i: The orthogonalized Craig-Bampton modes

L: The Lagrangian

F: The energy dissipation function

Ψ: The constraint equations

λ: The Lagrange multipliers for the constraints

ξ: The generalized coordinates

Q: the generalized applied forces ,the applied forces projected on ξ

d_{ij}: The damping coefficients

c_i: The modal damping ratio

c_i^{cr}: The critical damping ratio

m_i: The generalized mass

k_i: The generalized stiffness

η_i: Is referred to as CRATIO in the ADAMS dataset

1   INTRODUCTION

The prediction of pump and motor performance for a given design is essential for solving many practical problems and requires building a model that describe the flow of a viscous fluid, the torque and forces generated through the motion of the pump or motor. This computational process, where a model is built, is then simulated with the help of software packages in order to avoid the trial and error process based on long-term experience. Beside that, the continuing enhancement in the computer industry offers a great potential for more complex design models to be analyzed virtually. This research work investigates Parker-Hannifin Corp. new piston pump performance.

Chapter 2 presents a literature review of previous work in the piston pump industry and stresses on the findings that might be helpful while comparing them with the virtual analysis of the piston pump investigated. Most of the previous literature conducts a theoretical analysis using hydraulics theory followed by experimental results done in the labs. These results were validated with the virtual pump using software packages.

Chapter 3 deals with the rigid body analysis of the virtual pump. It is the static and dynamic analysis of the pump considering all its parts as rigid, i.e., there is no interaction between adjacent parts and there is no deformation of the parts due to the application of the loads on the parts. This analysis was conducted in order to get an overall estimate of the reactions on different moving

parts when the pump functions as one assembly connected by joints. Some of the parts experience high reactions (forces, moments and displacements) upon motion of the pump as a whole assembly. Therefore, a finite element analysis was conducted. This analysis is covered in Chapter 4, where the pistons, shaft, barrel and swash plate are considered. Each part was analyzed as being in static equilibrium, i.e., only input forces and displacement BCS were applied on the part. This analysis allows the designer to investigate the static behavior of the parts with severe initial loading conditions. Only critical components of the pump that were experiencing relatively high reactions were studied. In other words, by running the rigid body analysis, the parts that had high reaction forces were further analyzed by FEA in order to achieve the desirable strength of the parts with operation of the pump and to avoid failure. The finite element analysis concluded that the barrel was strong enough, while further analysis was deemed necessary on the shaft and pistons because they showed higher deformation than other parts. However, the swash plate also experienced high deformation, therefore it was redesigned with some geometry modification. The redesigned swash plate analysis revealed that it is strong enough and there is no need to conduct further analysis.

After studying the strength of the critical parts, a flex body analysis was conducted. This analysis is described in Chapter 5. The flex-body analysis considers the deformation and deflections of the parts upon the motion of the assembly. Flex-body simulation closely models the actual physical pump dynamics. The parts that showed the highest deflection in the finite element static

analysis were made as flexible parts in the overall assembly of the pump and simulation was conducted. The flex body analysis allows the designer to include the dynamic effects due to rotational motion of the pump on the desired parts made as flexible part. Moreover, it allows the designer to study regions of "hot spots" due to motion of the full assembly and plot the stress, strain distribution and the different frequencies or mode shape of vibration. The flex-body analysis aims to simulate the real pump tested in a laboratory.

Then, a discussion and comparison between the rigid body and the flexible body is presented. The results were interpreted and some parameters were validated with theoretical calculations. The flex body is a more advanced way of analyzing pumps or any moving assembly and gives results that match the theoretical ones.

In Chapter 6 a conclusion about the validity of the design is made. The results of the flex body analysis showed as follows; the piston has a reasonable deflection upon dynamic study and the deformation is not far from the static analysis conducted through finite element. Similarly, the shaft experiences a relatively low deformation upon the motion of the pump and the results are similar as the ones found in Chapter 4. The model designed and investigated was safe and can operate under normal conditions without failure.

Chapter 7 lists the references that were used while conducting the present work and writing this thesis.

The review of Literature

2.1 Introduction

This chapter mainly focuses on the theoretical aspect of piston pumps because limited research concerning virtual prototyping of piston pumps using MSC.ADAMS® is reported. Moreover, flex theory is briefly discussed. This theory is used for the development of the code used by ADAMS/FLEX.

The concept of piston pumps is defined in hydraulics books (Ref.10) as follows; the piston pump works on the principle of a reciprocating piston that can draw in fluid when it extends outward in a barrel or cylinder bore and discharge it when it retracts back into the barrel. There are two types of piston pumps one axial and the other is the radial design. Axial piston pumps have their pistons parallel to the axis of the cylinder block and can be either of bent axis configuration or of the swash plate design. Our main concern is in the axial piston pump with the swash plate design. One of the advantages of axial piston pumps is that of variable output displacement, i.e., given constant input speed and adequate power; axial pumps can effectively develop constant pressure and completely variable output.

The operating concept of a piston pump is based upon rotating a barrel against an angled swash plate. By controlling the angle of the swash plate, the output displacement is controlled and as a result, the output pressure varies. Axial pistons pumps are used in heavy-duty equipment, like tractors and

industrial applications, where there is a need for high output pressure in comparison to relatively lower pressure of the tank.

2.2 Governing Equations and Past Research

Ivantysyn (Ref. 2) has presented the analytic equations for pressure forces, centrifugal forces, and the friction forces on the piston, and the reaction force of the swash plate. For the free-body of the piston, k, shown in Figure 2.1 the instantaneous pressure force on piston k is given by:

$$F_{DK} = A_p \cdot (p_K) = \pi d_K^2 \cdot p_K / 4 \tag{1}$$

The inertia force of the piston with slippers is given by:

$$F_{aK} = m_K \cdot R \omega^2 \tan(\beta) \cos(\varphi) = F_{aKz} \tag{2}$$

Noting that,

$$F_{aKx} = F_{aKy} = 0 \tag{3}$$

And the centrifugal force acting on the piston is:

$$F_{\omega K} = m_K \cdot R \omega^2 \tag{4}$$

The components of this force are defined as follows:

$$F_{\omega Kx} = m_K \cdot R \omega^2 \sin\varphi \tag{5}$$

5

$$F_{\omega Ky} = m_K . R\omega^2 . \cos \varphi \qquad\qquad (6)$$

$$F_{\omega Kz} = 0 \qquad\qquad (7)$$
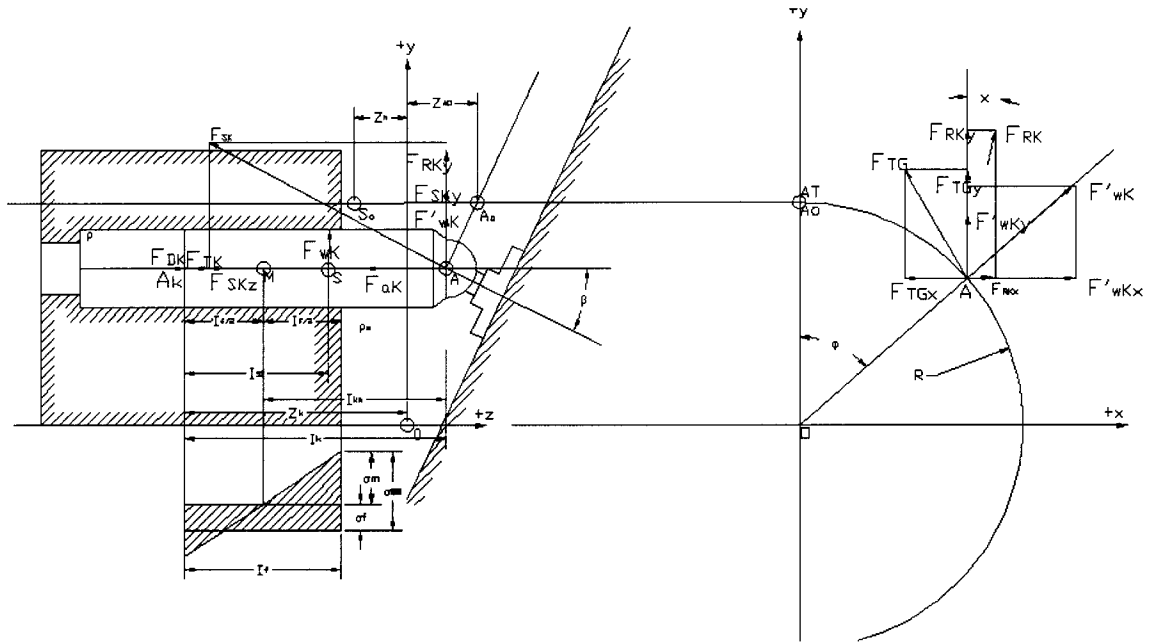
Figure 2.1: Free-body diagram of the piston with instantaneous forces

Furthermore, the total force acting on the piston is given by

$$F_{AK} = F_{DK} + F_{aK} + F_{TK} \qquad\qquad (8)$$

F_{TK} being the frictional force acting on the piston, which is insignificant, compared to the pressure force. The reaction force of the swash plate F_{SK} can be resolved in to three components:

$$F_{SKx} = 0; \; F_{SKy} = F'_{\omega K} + F_{RKy}; \; and \; F_{SKz} = F_{DK} + F_{TK} + F_{aK}$$

Where $F'_{\omega K}$ is the centrifugal force of the slipper.

Zeiger and Akers (Ref. 3) have studied the effects of variation in swash plate angular velocity and timing position of valve plate on torque on swash plate in piston pumps. According to their paper the resultant torque due to piston k occupying angle φ_k is given by:

$$T_j = PA_p \left(R\sin(\varphi_k) + a\sin(\varphi_k) + e\right)/\cos^2(\beta) \qquad (9)$$

where P is the pressure on the piston at the instant considered, A_p is the piston area, R is the piston pitch radius, a is the distance from the piston-slipper joint axis to the swash plate pivot, α is the swash plate angle, and e is the eccentricity of the swash plate pivot with respect to barrel pivot. The instantaneous torque (based on the geometrical relations shown in Figure 2.2) on the swash plate at any angular position of is given by

$$T(\varphi_k) = J_{RP}R\omega^2\tan(\beta) \quad +$$

$$\sum_{k=1}^{n} \left(PAp - m_K\omega^2 R\sin(\beta).\sin(\varphi_k)\right)\left(R\sin(\varphi_k) + a\sin\alpha + e\right)/\cos^2(\beta) \qquad (10)$$

where the summation is for k varying from 1 to n number of pistons, J_{RP} is the mass moment of inertia for the retainer plate. Thus the average torque, T_{av}, on the swash plate that has to be overcome by the control piston is obtained by integrating Equation (9) from 0 to $2\pi/n$ for each piston, summing the results of each integration, and dividing the result by $2\pi/n$. Zhang (Ref. 4) has generated the plots of theoretical control torque represented by Eq. (10). These plots could be used to compare the corresponding ADAMS results.
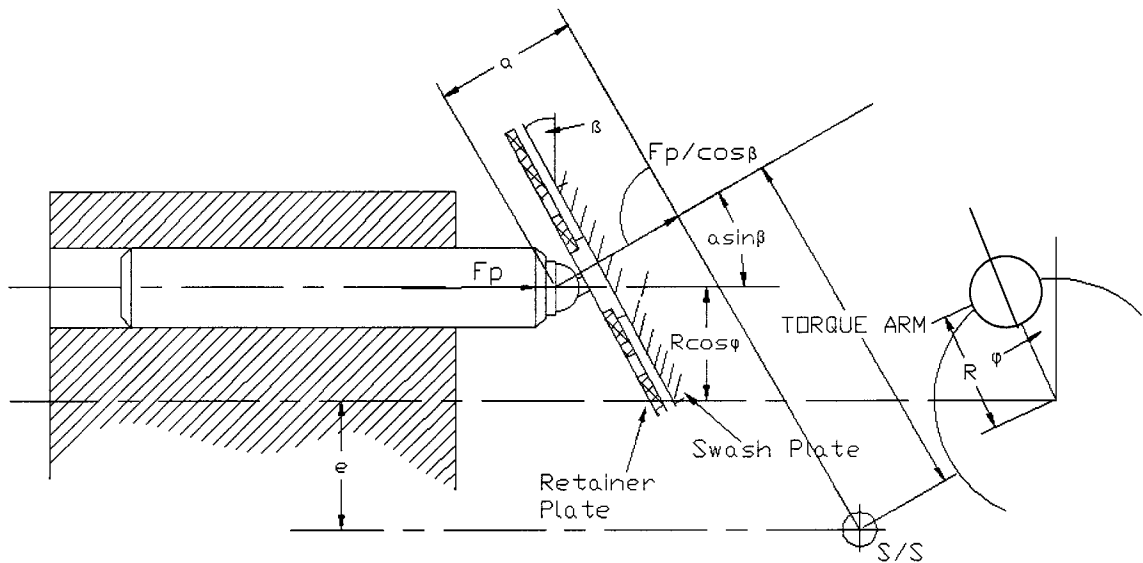
Figure 2.2: Geometrical relation of the piston, barrel, and swash plate (Ref. 3)

2.3 Flex body theory:

This section (Ref.8) gives the reader a working knowledge of the theory used to implement flexible bodies in ADAMS. The topics covered include:

- Modal superposition,

- Component mode synthesis,

- Mode shape orthonormalization,

- Flexible body equations of motion.

2.3.1 History of flexible bodies in ADAMS

MDI first attempted to automatically interface with Finite Element Method (FEM) software in a product called ADAMS/FEA. In ADAMS/FEA the FEM software used Guyan Reduction to automatically condense the entire set of FEM degrees of freedom (DOF) to a reduced number of DOF. In the Guyan reduction method, a set of user-defined master nodes are retained and the remaining set of

slave nodes are removed by condensation. Only stiffness properties are considered during the condensation, and inertia coupling of master and slave nodes are ignored. This is why Guyan reduction is sometimes referred to as static condensation. Guyan reduction condenses the large, sparse FEM mass and stiffness matrices down to a small, dense pair of matrices, with respect to the master DOF.

The challenge in ADAMS/FEA was to represent the master nodes using PART elements and an NFORCE element. While the condensed stiffness could be captured correctly by the NFORCE, the dense, condensed mass matrix from the Guyan reduction did not always lend itself to being represented by an "equivalent" lumped mass matrix. The goals of matching: total mass, center-of-mass location, moments of inertia, and natural frequencies could not always be met. ADAMS/FEA was difficult to use successfully and did not win favor with MDI's customers.

In 1996 MDI introduced an alternative modal flexibility method in a product called ADAMS/Flex. Rather than being based on ADAMS primitives like PART and NFORCE elements, ADAMS/Flex introduced a new inertia element, the Flex Body.

2.3.2 Modal superposition:

The single most important assumption behind the Flex Body is that we only consider small, linear body deformations relative to a local reference frame, while that local reference frame is undergoing large, non-linear global motion.

The discretization of a flexible component into a finite element model represents the infinite number of DOF with a finite, but very large number of finite elements DOF. The linear deformations of the nodes of this finite element mode, u, can be approximated as a linear combination of a smaller number of shape vectors (or mode shapes), Φ.

$$u = \sum_{i=1}^{M} \phi_i q_i \qquad (11)$$

Where M is the number of mode shape. The scale factors or amplitudes, q, are the modal coordinates.

A simple example of how a complex shape is built as a linear combination of simple shapes, illustrated as follows:

The basic premise of modal superposition is that the deformation behavior of a component with a very large number of nodal DOF can be captured with a much smaller number of modal DOF. We refer to this reduction in DOF as modal truncation.

Equation (11) is frequently presented in a matrix form:

$$u = \Phi q \qquad (12)$$

where q is the vector of modal coordinates and the modes Φ_i have been deposited in the columns of the modal matrix, Φ. After modal truncation Φ

becomes a rectangular matrix. The modal matrix Φ is the transformation from the small set of modal coordinates, q, to the larger set of physical coordinates u.

2.3.3 Mode shape orthonormalization:

The Craig-Bampton (Ref. 8) method is a powerful method for tailoring the modal basis to capture both the desired attachment effects and the desired level of dynamic content. However, the raw Craig-Bampton modal basis has certain deficiencies that make it unsuitable for direct use in a dynamic system simulation. These are:

1. Embedded in the Craig-Bampton constraint modes are six rigid body DOF that must be eliminated before the ADAMS analysis because ADAMS provides its own large-motion rigid body DOF.

2. The Craig-Bampton constraint modes are the result of a static condensation. Consequently, these modes do not advertise the dynamic frequency content that they must contribute to the flexible body. Successful simulation of a non-linear system with unknown frequency content is unlikely.

3. Craig-Bampton constraint modes cannot be disabled because to do so would be equivalent to applying a constraint on the system.

These problems with the raw Craig-Bampton modal basis are all resolved by applying a simple mathematical operation on the Craig-Bampton modes.

The Craig-Bampton modes are not an orthogonal set of modes, as evidenced by the fact that their generalized stiffness and mass matrices $\hat{K}$ and $\hat{M}$, are not diagonal.

$$\hat{K} = \Phi^T K \Phi = \begin{bmatrix} I & 0 \\ \Phi_{IC} & \Phi_{IN} \end{bmatrix}^T \begin{bmatrix} K_{BB} & K_{BI} \\ K_{IB} & K_{II} \end{bmatrix} \begin{bmatrix} I & 0 \\ \Phi_{IC} & \Phi_{IN} \end{bmatrix}$$

$$= \begin{bmatrix} \hat{K}_{CC} & 0 \\ 0 & \hat{K}_{NN} \end{bmatrix}$$

(13)

While the mass transformation is:

$$\hat{M} = \Phi^T M \Phi = \begin{bmatrix} I & 0 \\ \Phi_{IC} & \Phi_{IN} \end{bmatrix}^T \begin{bmatrix} M_{BB} & M_{BI} \\ M_{IB} & M_{II} \end{bmatrix} \begin{bmatrix} I & 0 \\ \Phi_{IC} & \Phi_{IN} \end{bmatrix}$$

$$= \begin{bmatrix} \hat{M}_{CC} & \hat{M}_{NC} \\ \hat{M}_{CN} & \hat{M}_{NN} \end{bmatrix}$$

(14)

By solving an eigenvalue problem

$$\hat{K} q = \lambda \hat{M} q$$ (15)

We obtain eigenvectors that we arrange in a transformation matrix N, which transforms the Craig-Bampton modal basis to an equivalent, orthogonal basis with modal coordinates q^*,

$$N q^* = q$$ (16)

The effect on the superposition formula is

$$u = \sum_{i=1}^{M} \phi_i q_i = \sum_{i=1}^{M} \phi_i N q^* = \sum_{i=1}^{M} \phi_i^* q^*$$ (17)

where ϕ_i^* are the orthogonalized Craig-Bampton modes.

The orthogonalized Craig-Bampton modes are not eigenvectors of the original system. They are eigenvectors of the Craig-Bampton representation of the system and as such have a natural frequency associated with them. A physical description of these modes is difficult, but in general the following is observed:

- Fixed-boundary normal modes are replaced with an approximation of the eigenvectors of the unconstrained body. This is an approximation because it is based only on the Craig-Bampton modes. Out of these modes, 6 modes are usually the rigid body modes.

- Constraint modes are replaced with boundary eigenvector, a concept best illustrated by comparing the modes before and after orthogonalization of a rectangular plate which has Craig-Bampton attachment points along one of its long edges. The Craig-Bampton mode in Figure 2.3 features a unit displacement of one of its edge nodes with all the other nodes along that edge fixed. After orthonormalization we see modes like the one depicted in Figure 2.4, which has a sinusoidal curve along the boundary edge.
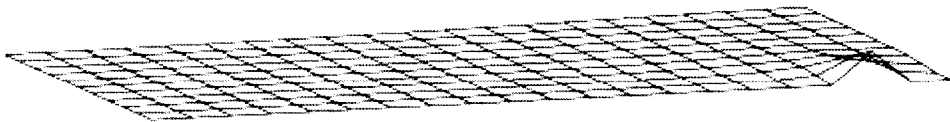
Figure 2.3: Constraint mode with an unknown frequency contribution

Figure 2.4: Boundary eigenvector with a 1250 Hz natural frequency.

- Finally, there are modes in a gray area between the first two sets that defy physical classification.

We conclude that the orthonormalization of the Craig-Bampton modes addresses the problems identified earlier, because:

1. Orthonormalization yields the modes of the unconstrained system, six of which are rigid body modes, which can now be disabled.

2. Following the second eigensolution, all modes have an associated natural frequency. Problems arising from modes contributing high-frequency content can now be anticipated.

3. Although the removal of any mode constrains the body from adopting that particular shape, the removal of a high-frequency mode such as the one depicted in Figure 2.4 is clearly more benign than removing the mode depicted in Figure 2.3. The removal of the latter mode prevents the associated boundary node from moving relative to its neighbors. Meanwhile, the removal of the former mode only prevents boundary edge from reaching this degree of "waviness".

2.3.4 Flexible body equations of motion:

The governing equations for a flexible body are derived from Lagrange's equations of the form:

$$\frac{d}{dt}\left(\frac{\partial L}{\partial \dot{\xi}}\right) - \frac{\partial L}{\partial \xi} + \frac{\partial F}{\partial \dot{\xi}} + \left[\frac{\partial \Psi}{\partial \xi}\right]^T \lambda - Q = 0 \qquad (18)$$

$$\Psi = 0 \qquad (19)$$

where,

L is the Lagrangian, defined below

F is an energy dissipation function, defined below

Ψ are the constraint equations

λ are the Lagrange multipliers for the constraints

ξ are the generalized coordinates as defined in the following equation

Q is the generalized applied forces (the applied forces projected on ξ)

$$\xi = \begin{Bmatrix} x \\ y \\ z \\ \psi \\ \theta \\ \phi \\ q_{i(i=1....M)} \end{Bmatrix} = \begin{Bmatrix} X \\ \psi \\ q \end{Bmatrix} \qquad (20)$$

The Lagrangian is defined as

$$L = T - V$$

where T and V denote kinetic and potential energy respectively.

2.3.5 Dissipation and the damping matrix:

The damping forces depend on the generalized modal velocities and are assumed to be derivable from the quadratic form

$$F = \frac{1}{2} \dot{q}^T D \dot{q} \qquad (21)$$

which is known as Rayleigh's dissipation function. The matrix D contains the damping coefficients, d_{ij}, and is generally constant and symmetric.

In the case of orthogonal mode shapes, the damping matrix can be effectively defined using a diagonal matrix of modal damping ratios, c_i. This damping ratio could be different for each of the orthogonal modes and can be conveniently defined as a critical damping for the mode, c_i^{cr}. Recall that the critical damping

ratio is defined as the level of damping that eliminates harmonic response as seen in the following derivation.

Consider the simple harmonic oscillator defined by uncoupled mode i.

$$m_i \ddot{q}_i + c_i \dot{q}_i + k_i q_i = 0 \qquad (22)$$

where m_i, k_i and c_i denote, respectively, the generalized mass, the generalized stiffness, and the modal damping corresponding to mode i.

Assuming the solution $q_i = e^{\lambda t}$, leads to a characteristic equation

$$m_i \lambda^2 + c_i \lambda + k_i = 0 \qquad (23)$$

which has the solution

$$\lambda = \frac{-c_i \pm j\sqrt{4m_i k_i - c_i^2}}{2m_i} \qquad (24)$$

The critical damping of mode i, is the one that eliminates the imaginary part of λ

$$c_i^{cr} = 2\sqrt{k_i m_i} \qquad (25)$$

Defining c_i as a ratio of critical damping introduces the modal damping ratio, η_i, which is referred to as CRATIO in the ADAMS dataset.

$$c_i = \eta_i c_i^{cr} \qquad (26)$$

The solution to Eq. (22) is

$$q_i = e^{-\eta_i \sqrt{\frac{k_i}{m_i}} t} e^{j\left(\sqrt{(1-\eta^2)}\omega_i t\right)} \qquad (27)$$

16

where $\omega_i = \sqrt{\dfrac{k_i}{m_i}}$ is the natural frequency of the undamped system. This solution

ceases to be harmonic when $\eta_i = 1$, which corresponds to 100% of critical

damping.

The Rigid Body Analysis

3.1 Introduction:

Computer softwares are getting more and more powerful in solving complex engineering problems. This chapter describes the rigid body modeling of the piston pump investigated. The rigid body analysis involves studying the dynamics of the pump such as the forces and reactions upon the motion of the pump. Therefore this analysis is done in order to get as much information about the pump and its components. Having these results, one can then go a further step and analyze the parts that exhibit high forces and reactions upon the motion of the whole assembly in order to assist the design process and eliminate the shortcomings of the design.

3.2 Procedure:

The objective is to model a piston pump for a specified swash plate angle, shaft rotational speed of 2500 rev/min, and the pressure profiles provided by Parker design engineers, and to analyze some of the critical variables, such as the pressure forces on the pistons, the force and torque on the actuator piston, and the contact and friction forces between the piston-barrel interface. This piston pump consists of many components connected together in order to get the desired assembly.

As mentioned previously, this chapter consists of a rigid-multi-body simulation. The task was to simulate the motion of the rotary group of the Parker pump. Automatic Dynamic Analysis Mechanism software-MSC.ADAMS®, in conjunction with Pro/Engineer, PRO/E®, helped the seamless export of solid model pump file of PRO/E® into MSC.ADAMS®. The export through MECH/PRO®, an MSC.ADAMS® module in PRO/E® environment, maintained the kinematics, inertial, and material properties of the pump components. Thus significant time was saved, as there was no need to manually input the properties of tens of components. Some time was spent to acquire the knowledge of piston pump technology and simulation software training. Then the work began on ADAMS/View by connecting the different parts of the piston pump together to create a rigid body. Different types of joints were used between the moving and fixed parts: Revolute joints, Cylindrical joints, Translational joints, Fixed joints, Planar joints, and Spherical joints that allow rotation about all three axes.

Figure 3.1: The piston pump prototype

Additionally, the pressure profiles provided by Parker were input through the AKIMA function of ADAMS for the nine pistons that each lagged the previous piston by 40°. Figure 3.2 illustrate the mapping of the pistons at a specific time where the 360° is divided into 9 parts and the result is 40° lag between each piston.

BDC
90
deg.

Pc – cylinder with generated pressure curve.

FiLookat

180 deg.

TDC
270
deg.
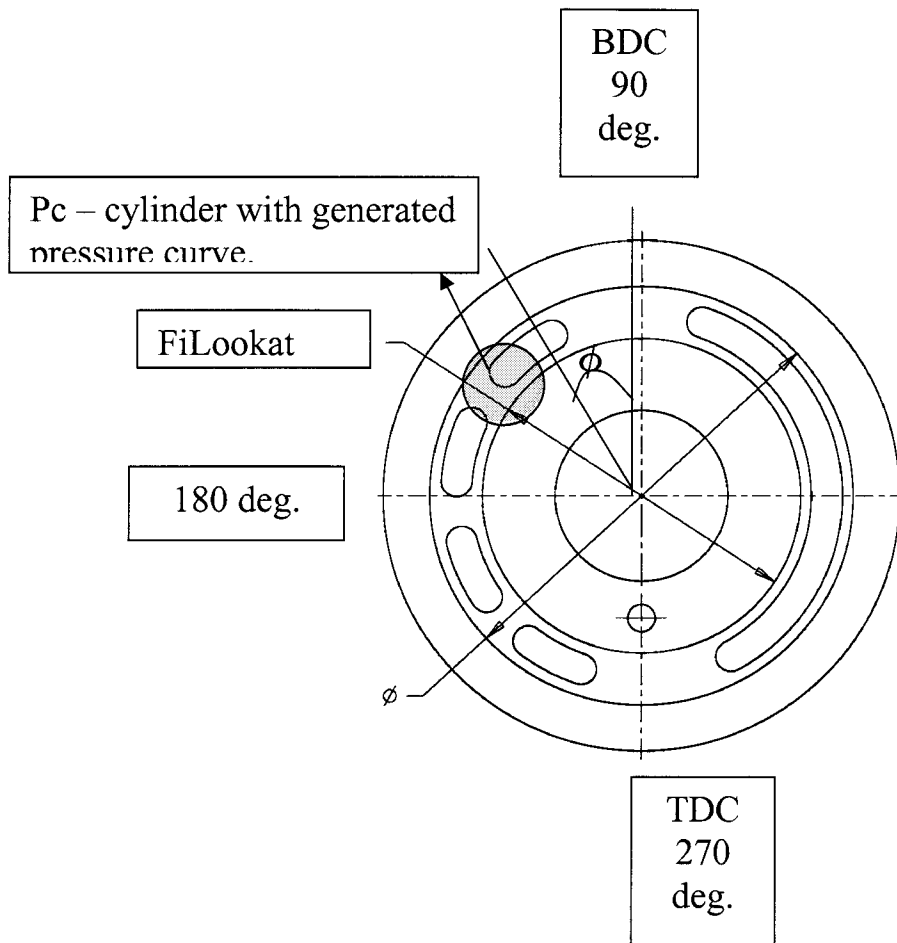
Figure 3.2: Definition of piston angular position

Once the pressure profile was set up, the next step was to introduce friction force between the pistons and the barrel. Therefore, the static and dynamic friction factors were changed for each translational joint connecting the pistons and the barrel; the μ_{static} =0.2 and $\mu_{dynamic}$ =0.05. Friction was modeled as dry. Next, contact forces were added between each shoe and the slipper retainer plate in order to model the realistic motion. After doing so and activating all the forces from pressure profile to friction to contact forces the simulation was run. This piston pump design is studied for the operating pressure range of between 30 and 42MPa at the maximum specified swash angle. Thus the MSC.ADAMS®

models were built and simulated per the following matrix in Table 3.1, showing the number of simulations runs for some key parametric changes. The discussion below highlights analysis of results for output pressure of 42MPa.

Table 3.1: Matrix of simulation runs

Run No.	Output pressure MPa	Shaft Speed RPM	Swash Plate Angle Degrees	All Contact Forces Off or On
1	42	2500	23	Off
2	42	2500	23	On
3	30	2500	23	Off
4	30	2500	23	On

A typical ADAMS model excludes the parts that are not critical to this analysis, such as pump casing, left-hand block, shaft bearings, etc. These parts were deactivated in order to simplify the model dealt with and to avoid unnecessary software calculation throughout the simulation.

3.3 Analysis and Discussion:

After setting up the model and connecting all parts together, and checking the inputs, the simulation was ready to run.

We will begin with the input force, which is 12500N calculated as follows:

$$F_{DK} = A_p (P_K)$$

$$= (298*10^{-6} \text{ m}^2)*(42*10^6 \text{ N/m}^2)$$

$$= 12516 \text{ N}.$$

Note that the input is a force that acts at the center of gravity of the piston and this force is the reaction of the pressure input of 42MPa. MSC.ADAMS® does not

accept pressure; therefore the pressure was transformed into a moving force by multiplying it with the desired area.

Figure 3.3 shows the pressure forces as an input for a randomly chosen piston 2, 3 and 4. They are step forces acting only for a period of time and they are shifted by a 40° angle. Their maximum absolute value is 12500N.
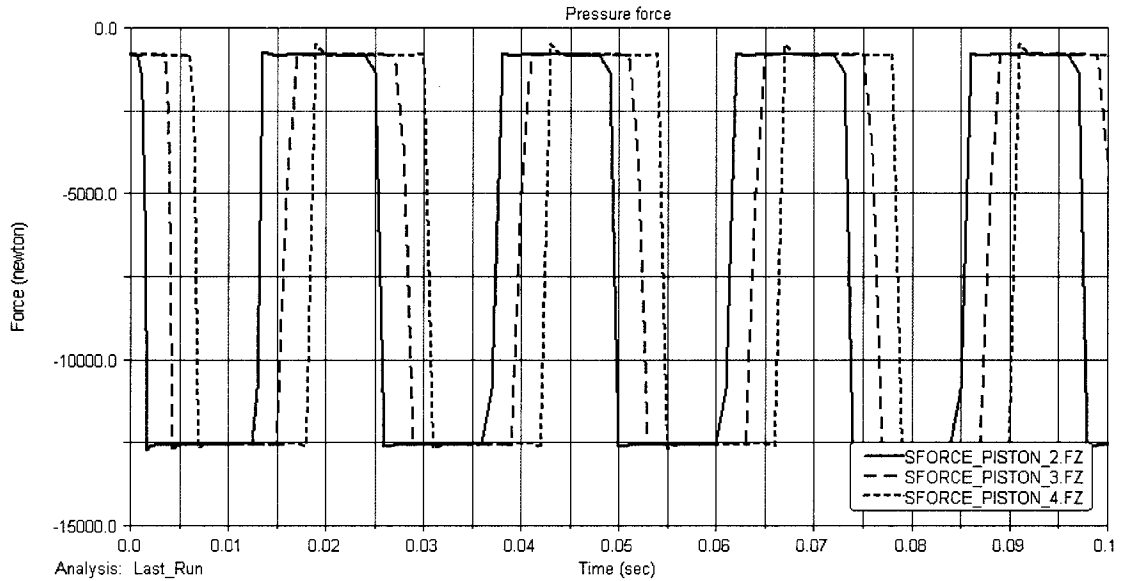
Figure 3.3: Pressure force for rigid body simulation

Plotting the forces with respect to the rotation angle shows us the pressure distribution at different locations. Figure 3.4 below illustrates this idea for rigid body simulation, where the 40° lag angle is clearly shown here. In other word, piston 3 get the input pressure force of 12500N beginning at 225° till 390°, while piston 4 gets it 40° after, that is 265° till 430°. Notice that the input pressure data was superposed in the AKIMA function in order to insure that at least two revolutions of the pump were cover and further rotation will be a repetition of the profile. That is why the angles reach 720° in the Figures. Connecting the pressure profile to the angle position means that the pressure is a function of

position and not time, therefore, this allows us to run the simulation for a long time (i.e., revolutions) and knowing that the pressure repeats itself.
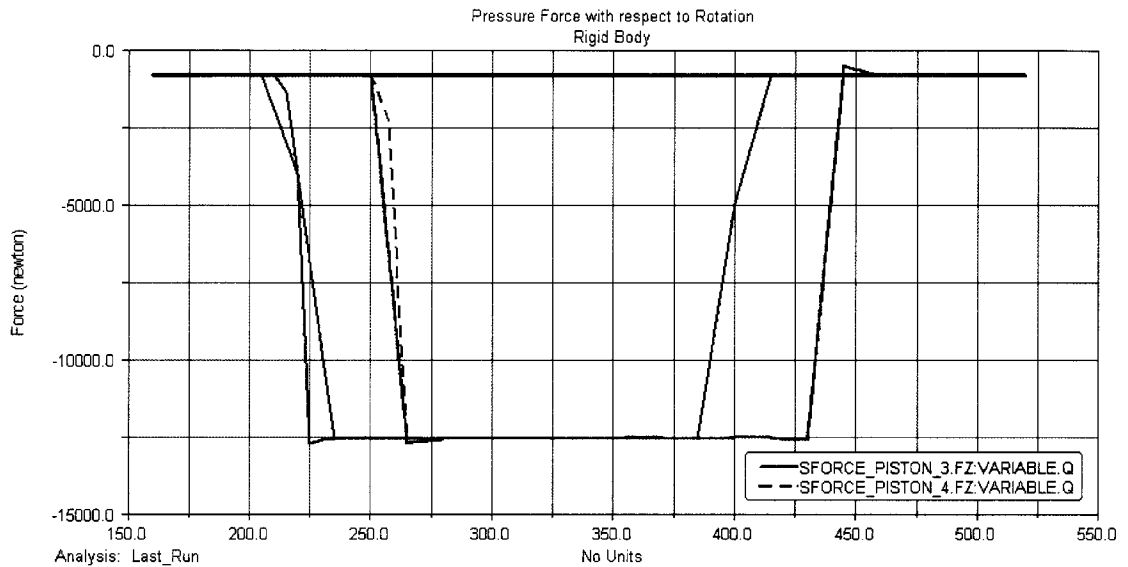
Figure 3.4: The pressure profile with respect to the angle of rotation for rigid body

The angle mapping for each piston locates its position with respect to the rotation of the shaft (rpm) is shown in Figure 3.5. Each angle covers 360° per one revolution of the pump. And it is associated to a piston that ensures the location of this piston at different time. Notice the phase difference between two consecutive angles is 40°.

24
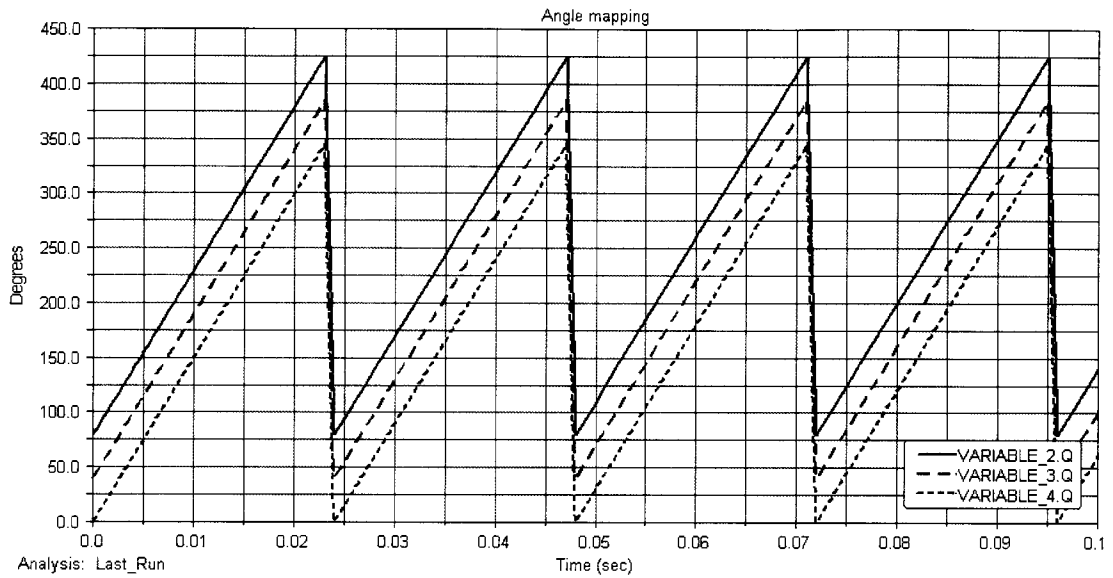
Figure 3.5: The angle mapping for the rigid body simulation

Forces between the pistons and the barrel are also investigated because they are important for the design and give ideas about what is happening in the interaction between the piston and the barrel (or sleeves). This is illustrated in Figure 3.6; and again joints 2, 3 and 4 were randomly chosen.
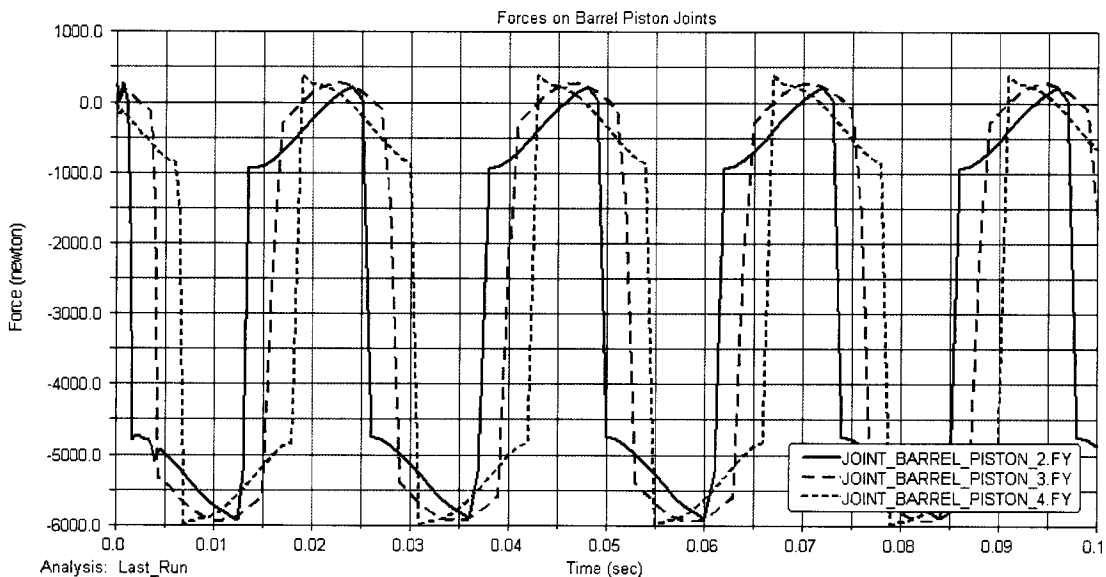
Figure 3.6: Forces on the barrel piston joint in the Y-direction for rigid body simulation
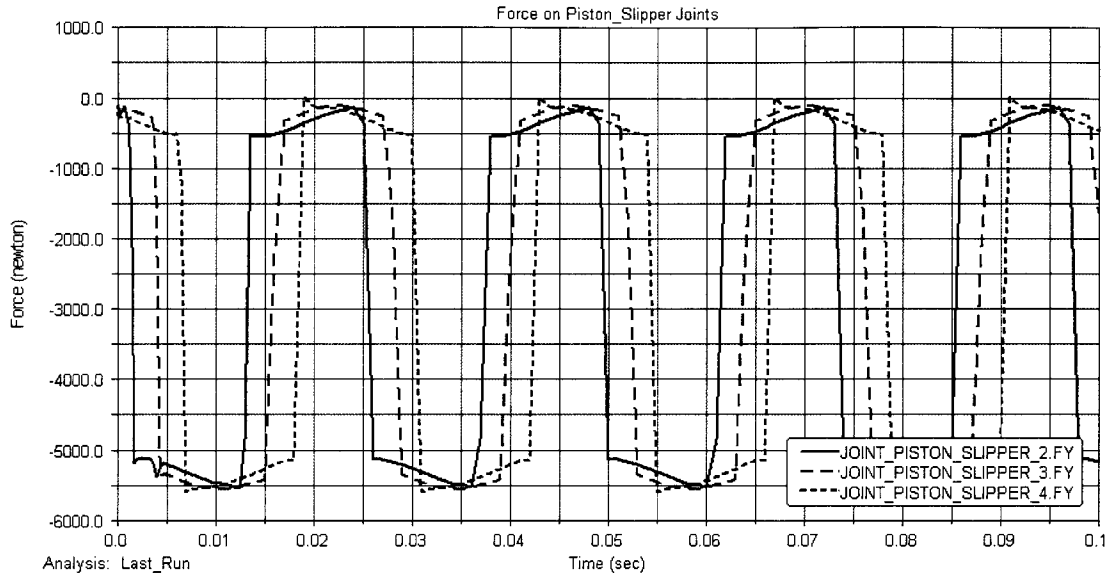
Figure 3.7: Forces on the piston slipper joint in the Y-direction for rigid body simulation

Similarly, Figure 3.7 shows the forces between the piston and slipper interface. These values are found to be equal and opposite of the forces on the swash and slipper interface, which are illustrated in Figure 3.8. The maximum value is of 5500N. These values are expected to be equal and opposite because of the action-reaction concept. The forces resulting from the applied pressure on the pistons are transmitted through the slippers into the swash plate. In the model joints connecting the pistons to the slippers and the later to the swash plate carry these forces.
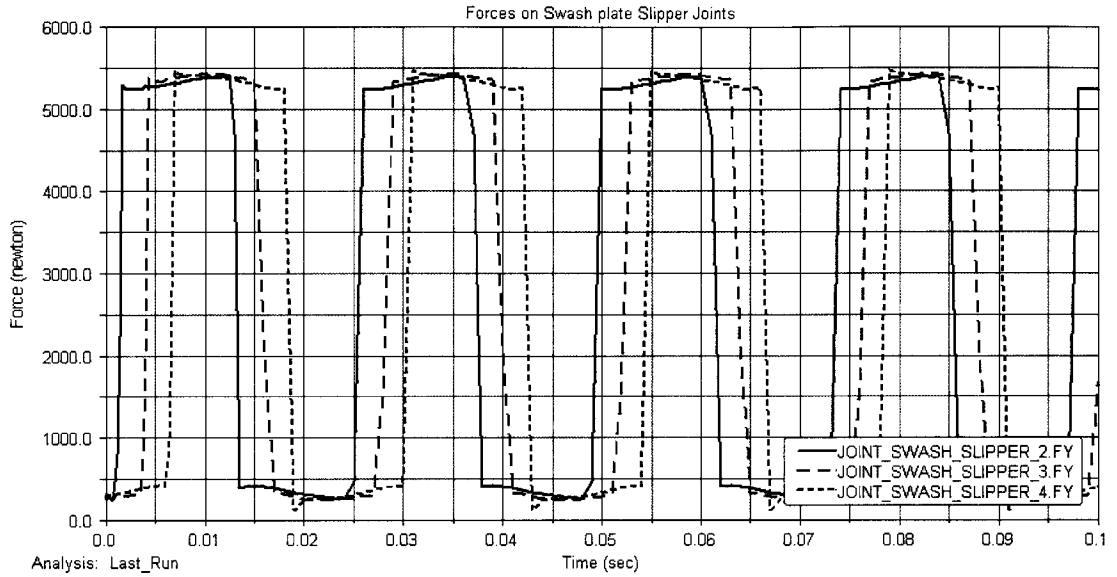
Figure 3.8: Forces on the swash plate slipper Joint in the Y-direction for rigid body simulation

Figure 3.9 illustrates the force applied on the shaft due to the operation of the pump. The input pressure on the pistons mainly generates this force where some of the reaction is transmitted through the barrel and in its turn the barrel exerted a force on the splines where it is connected to the shaft.
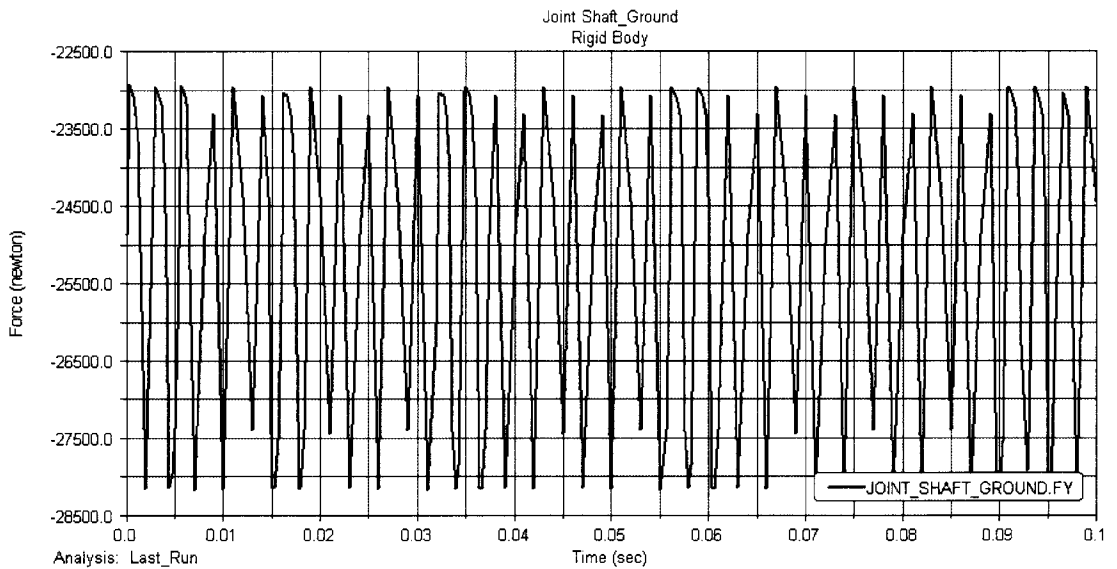
Figure 3.9: Forces on the shaft ground joint in the Y-direction for rigid body simulation

Notice that the average value of the force on the joint between the shaft and ground in the y direction for this rigid body simulation is -25248.29N. While the maximum and minimum values are -22917.32N and -28170.07N respectively. To be mentioned that the sign here does not matter because it can be changed by flipping the choice between the first and the second marker when measuring. The rigid body center of mass of the shaft is shown in Figure 3.10 below:
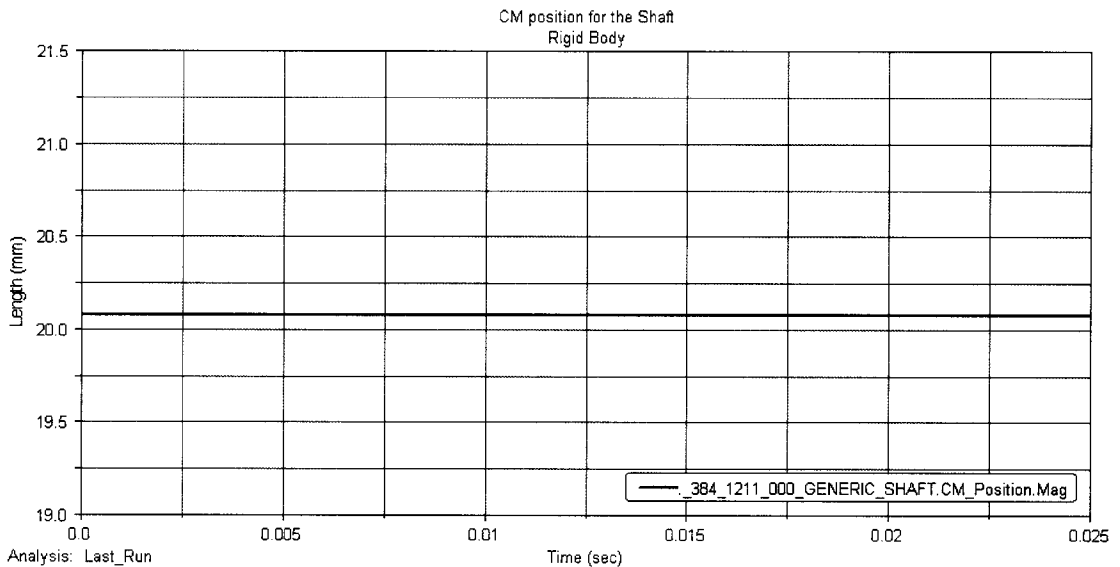
Figure 3.10: The center of mass of the shaft for rigid body simulation

Notice that the center of mass for the shaft being as a rigid body is constant and does not change, which is expected because the shaft is not supposed to deflect. Its value is 20.08mm.

We investigate the angular kinetic energy of the shaft for the rigid body simulation and using theoretical calculation validates the results. The kinetic energy of the shaft might be useful because it can give an idea about the amount of energy that can be lost through heat dissipation and how it can contaminate the working fluid of the pump.

The kinetic energy for the shaft using rigid body simulation is shown in Figure 3.11 below:
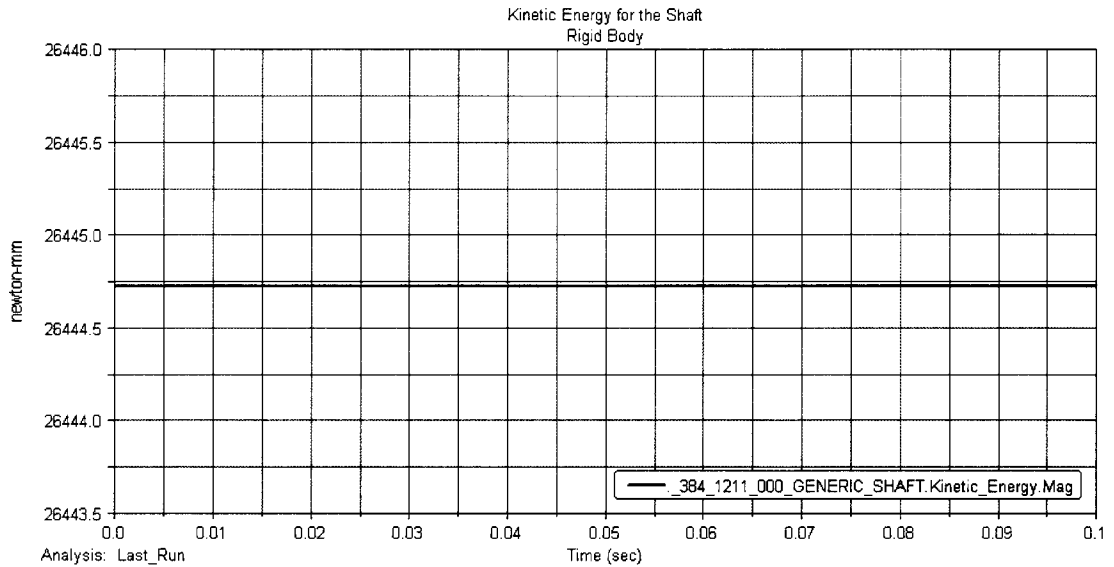
Figure 3.11: kinetic energy for the shaft rigid body simulation

The angular kinetic energy of the shaft is validated by using hand calculation as follows. The mass of the shaft is m_{shaft}= 3.4651566 Kg and the radius is about R = 15mm with the angular velocity of 2500rev/min, using the following we get:

$$KE = \frac{1}{2}(m)(R\omega)^2$$

$$KE = \frac{1}{2}(3.4651566kg)\left(\frac{(15\times10^{-3}m)\times2500\times2\pi}{60\sec}\right)^2\left(\frac{1000mm}{1m}\right)$$

= **26718.535N.mm**

Notice that the angular kinetic energy for the shaft with the rigid body simulation is constant and equal to **26444.700N.mm.** This value is constant as expected because the shaft is not supposed to deflect or deform with the rigid

29

body simulation. Comparing this value with the theoretical calculation above we see that the error is around 1% for this rigid body simulation.

Similarly, the angular kinetic energy of one of the pistons is investigated for the rigid body simulation and the results are validated by using theoretical calculation.

The kinetic energy for piston 2 using rigid body simulation is shown in Figure 3.12:
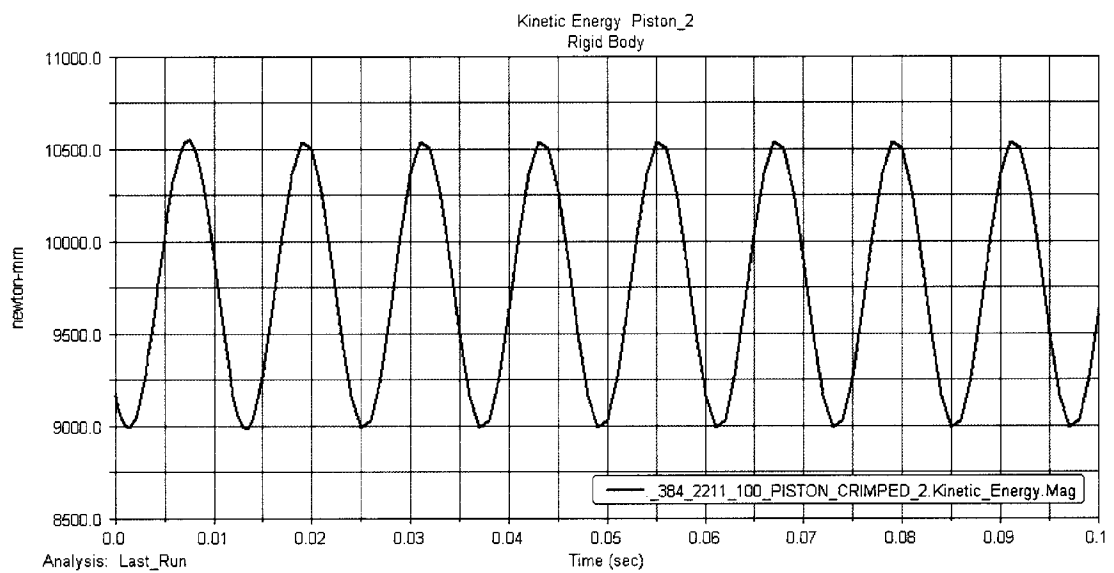
Figure 3.12: kinetic energy for piston 2 rigid body simulation

The theoretical calculation of the angular kinetic energy of the piston is validated by using hand calculation as follows. The mass of the piston is m_{piston}= 0.12801098 Kg and the radius is about R = 46mm with the angular velocity of 2500rev/min, using the following we get:

$$KE = \frac{1}{2}(m)(R\omega)^2$$

$$KE = \frac{1}{2}(0.12801098kg)\left(\frac{\left(46\times10^{-3}\,m\right)\times2500\times2\pi}{60\sec}\right)^{2}\left(\frac{1000mm}{1m}\right)$$

= **9282.61N.mm**

Notice that the angular kinetic energy for the piston with the rigid body simulation is has an average value of **9710.79N.mm.** This value is oscillating between 9000N.mm and 10548N.mm as expected because the piston is moving back and forth and undergoing a periodic motion. Comparing these values with the theoretical calculation above we see that the error is around 4.4% for the rigid body simulation. The results are close to the theoretical calculation.

Figure 3.13 below shows the contact forces between the slippers and the retraction plate. The main reason for the motion of the retraction plate is the contact forces modeled between this plate and the slippers. These contact forces are investigated in order to check if the design of the slippers is safe.
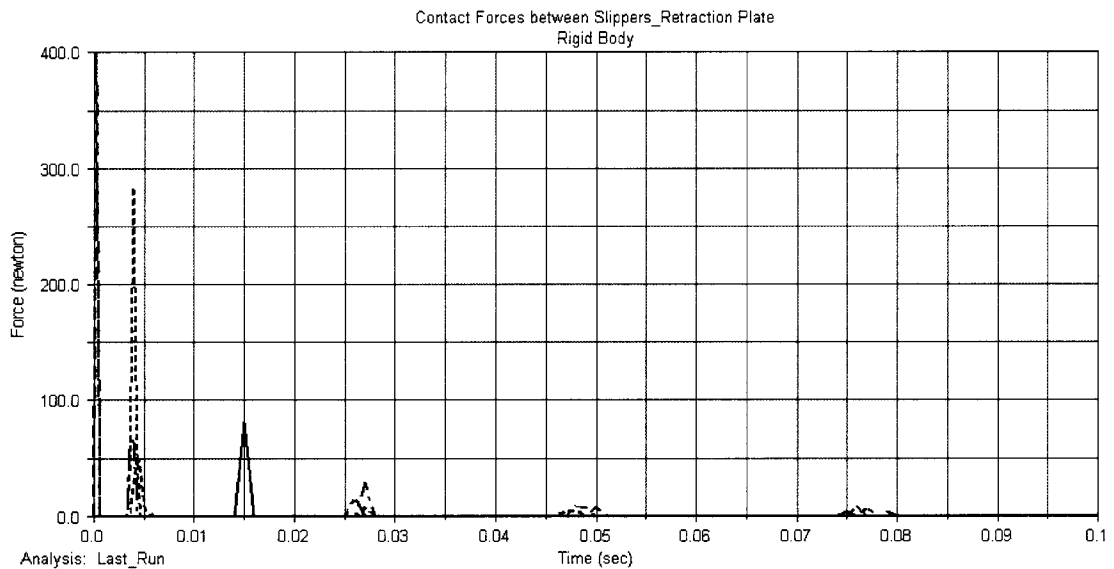
Figure 3.13: Contact forces between the slippers and retraction plate for rigid body simulation

Notice that the contact forces between the slippers and the retraction plate are in a reasonable range, where the highest value is around 400N. These predicted values are in good agreement to the experimental results from Parker.

Then, the contact forces between the pistons and the sleeves were found and are shown in Figure 3.14 below:
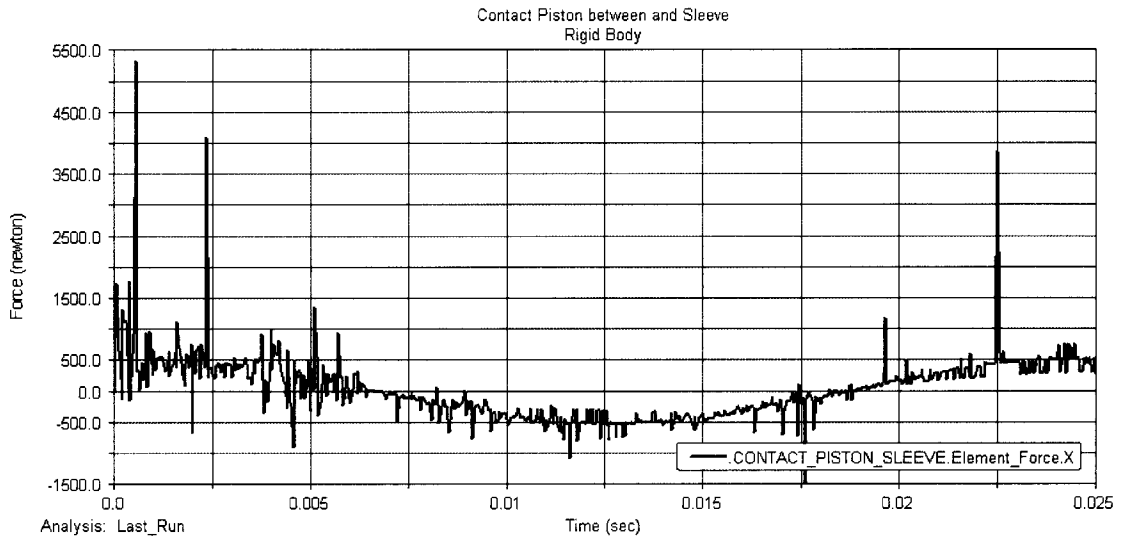
Figure 3.14: Contact forces between the pistons and sleeves for rigid body simulation

Notice that the contact force has a maximum value of 5327.24N and a minimum value of -1499.98N. These values are not in a critical range keeping in mind that the contact that we modeled is a dry contact with no lubrication that minimizes the contact force and friction.

Figure 3.15 illustrates the moment on the swash plate due to the operation of the pump. The X and Y components are shown and the maximum and minimum values are listed in the following Table:

Table 3.2: The swash plate moment in the X- and Y-direction:

Simulation	Rigid body	
Value	Max	Min
T_x (Nmm)	1.721×10^6	-1.804×10^6
T_y (Nmm)	1.822×10^6	-1.208×10^6
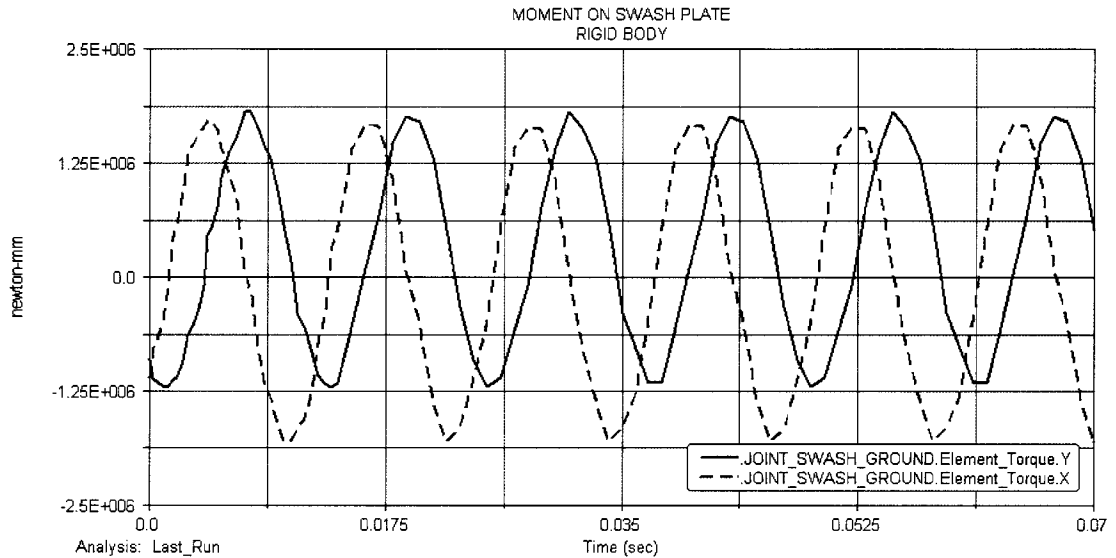
Figure 3.15: The moment on the swash plate for rigid body simulation

3.4 Summary of Chapter 3:

The rigid body simulation was successful, and the results obtained helped us to determine the critical parts in the assembly for more in-depth analysis. These parts are the piston, shaft, and barrel and swash plate. Upon operation of the pump, these parts experience high forces that may lead to failure after repetitive operation, therefore, the choice of performing finite element analysis on these parts was made in order to create a safer design and avoid premature failure.

Due to the high pressure input through the pistons, an analysis should be made of the pistons in order to avoid deformation and failure operation. There were two concerns; the first is the forces transmitted through the sleeves that directly affect the barrel and the lateral deflection of the pistons. These are shown in Figure 3.6 and having a value of 6000N. These forces may also deform the sleeves (bushings) and can wear the metal-to-metal contact and create leakage from the pistons. The second concern was the forces that are transmitted through the slippers (Figure 3.7) and the reaction from these slippers creating a force at the tip of the piston that may bend the piston and create forces at the point of contact between the piston and the sleeves, because once bent, the contact between the piston and sleeve will not remain as a surface contact but there will be a concentrated force and the end of the piston that may wear the sleeve quickly.

On the other hand, the forces that were transmitted through the slippers will act on the swash plate (Figure 3.8) and may cause deformation of that swash plate or may wear the bearing between the swash plate and the casing. These forces were found to be 5500N from each slipper.

The forces on the shaft having an average value of 25248.29N (Figure 3.9) were concentrated on the splines connecting it with the barrel and are the result of the pressure in the pistons that push the barrel in the Y-direction creating a reaction on the shaft that deform it and may cause failure.

Due to the fact that the barrel is connected to the shaft and it hold the piston, therefore, the barrel was also considered as a critical part and needed further analysis.

Based on these findings and conclusions, the critical parts considered were analysis using finite element. This is discussed in Chapter 4.

Finite Element Analysis:

4.1 Introduction:

After running the rigid body simulation, some of the findings were investigated. There are some of the parts that experience high forces and reactions. In order to make sure that these parts were a safe design and do not experience failure after short-term use, a Finite Element Analysis (FEA) was considered (Ref.9). The parts that are of interest are the barrel, piston, shaft, and swash plate. These parts were analyzed using the MSC.NASTRAN$^{®}$ software. The Finite Element Analysis treats the loads as being static and gives a pretty good indication of the strength of the parts.

For more details about the compete Finite Element Analysis one can refer to "Modeling and Virtual Prototyping of Parker-Hannifin's Piston Pumps, Report Phase II, March 2004".

4.2 Objective:

The components analyzed were the barrel, piston, shaft, and swash plate. The pistons in a piston pump are subjected extremely high compressive forces, F_P, generated due to high pump output pressure of 42MPa and potentially high bending forces, F_B. Figure 4.1 show compressive, bending, and resultant forces, F_P, F_B, and F_R respectively on one of the pistons. The piston forces are transmitted to the swash plate through the slippers. The shaft has to withstand

the input, reaction due to barrel driving the pistons, and output torques. Static analysis was performed on the components cited above for the "worst-case" situation to determine if the maximum stresses predicted for the worst case exceeds yield strength of the material. Maximum deformations and regions where they occur were also studied. FEA was conducted using MSC.NASTRAN®, and pre and post-processing were done in MSC.PATRAN®.

Fixed at this
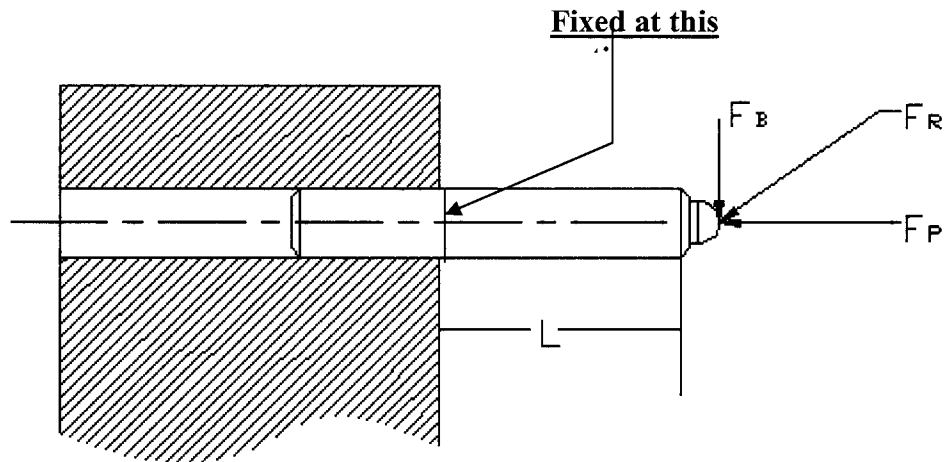
Figure 4.1: Forces on a piston

4.3 Procedure:

The applied loads and constraints to the components represent the worst-case scenario in static equilibrium. The resulting stresses and deformations thus could be construed as maximum that could be expected in the critical components. If any of these components exhibit stresses higher than the ultimate strength of the material then further investigation would be necessary. The pump is expected to operate at its maximum power for swash plate angle of $23°$, the shaft rotational speed of 2500 rev/min, and the output pressure of 42MPa. All the loads include a factor of safety as specified by Parker engineers.

The pistons were analyzed when it is at the maximum stroke when the forces are greatest at 13900N at 23° angle of the swash plate. The bending forces are greatest on the piston when it is at the bottom-dead-position of the stroke. Figures 4.2 and 4.3 show the various constraints and loads respectively.
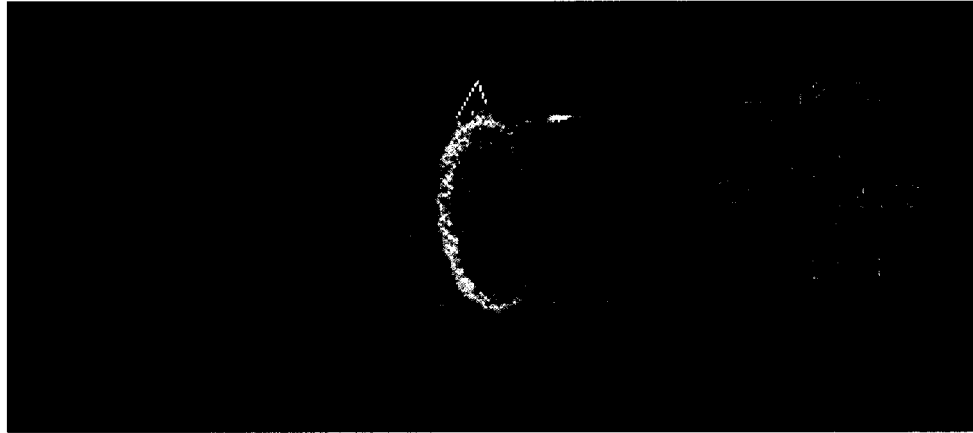
Figure 4.2: Constraints on the piston
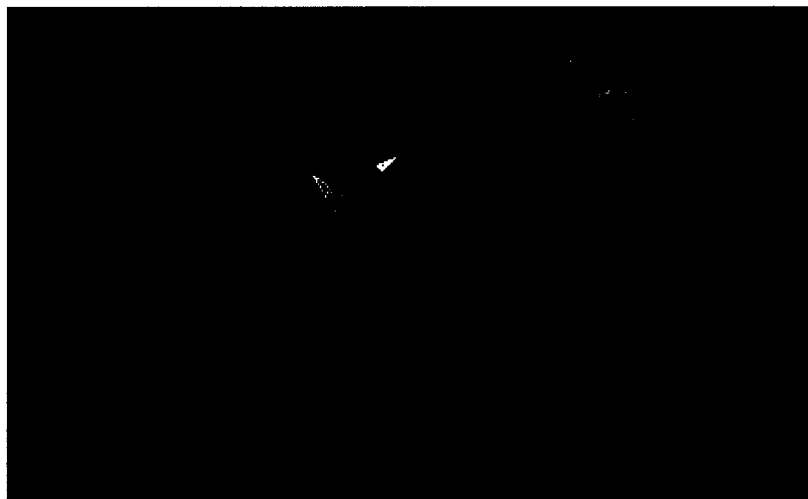
Figure 4.3: Loading on the piston

The pump components, in particular its shaft, are to be strong enough so that the pump can be connected in series to another identical pump at the output end of its shaft for higher output pressure and fluid power. Because of this, the input splines must withstand at least 2.5 times the barrel torque - maximum -

97250 Nm. The splines at the barrel deliver an equal and opposite to the rated fluid torque at the maximum operating conditions – flow rate, swash angle, angular speed, and output pressure. For FEA, the shaft is modeled to remain in static equilibrium with the output shaft absorbing the remaining torque, 57250 Nm. The torques are represented as forces acting tangentially to the pitch circle and perpendicular to the spline lateral surface for along half the circumference of the barrel splines, as shown in Figure 4.4. The forces are similarly applied as couples at the output and input ends of the shaft along the entire circumference of the pitch circles.

Figure 4.4: Loading on shaft model

The shaft is constrained at the bearings in all directions except for translational and rotational degree of freedom along the shaft axis. The shaft is also similarly constrained at the outer surface of the output end along its axis. This is illustrated in Figure 4.5.

Figure 4.5: Shaft constraints

The barrels are analyzed at worse case scenario, i.e., when four of the nine pistons are loaded to twice their maximum side load of 5000N, each acting tangentially on the barrel pitch circle on half the cylindrical surface of bore in the direction opposite to barrel rotation. The other half of the bore is constrained in all six degrees of freedom. The force is applied to the solid's elements on that line. The maximum piston force is created when maximum torque is being delivered to the barrel and is acting on half of the barrel splines. The torque is applied as a force acting tangentially on the face of the spline teeth as was done in the shaft model. This force remains the same as delivered by the shaft of 38900N. These forces are shown in the MSC.PATRAN® solid model below in Figure 4.6. The constraints to barrel motion are shown in Figure 4.7.

Figure 4.6: Barrel loads

Figure 4.7: Barrel constraints

The swash plate experiences transfer of the forces from each of the five pistons through slippers via the spherical ball joints attached to the pistons due to the high-pressure side of the cycle. As seen in Figure 4.8 the placement of the forces on the elements coincides with the axes of the slipper shoes. The swash plate for the original model was analyzed. Based on the results, it was

determined that the deformation characteristics were undesirable in that the swash plate has the tendency to deform excessively about the z-axis. The consequence of this would be to open up the clearance between the oil port on the swash and the bearing leading to oil leakage. To reduce the deformation the design engineers modified the geometry and the FEA was conducted for the changed geometry. Figures 4.9, 4.10 and 4.11 show the reaction forces and the constraints for the revised swash plate: the piston loads of 14767N are located along the slipper shoes axes on the contact plane of the swash plate. Two loads were placed on the rear bushings for equilibrium of the forces due to hydrostatic oil pressure to create a "floating" contact of the swash with bearing surface. The greater total load of 59905N was placed on the same side where the 5 piston forces contact. A load of 13995N was placed on the other side. The swash plate was constrained in the center along the inside of the bushings as can be seen in the Figure below. The other constraints were on the edges of the center hole that can be seen in Figure 4.11.
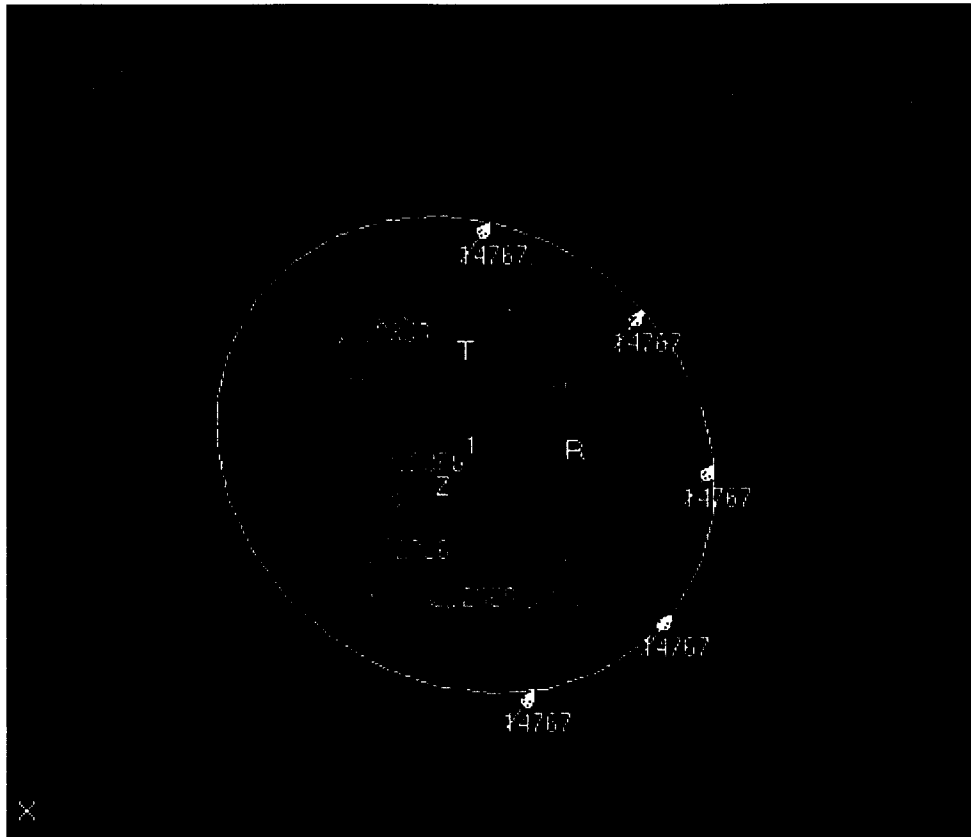
Figure 4.8: Swash plate piston loading
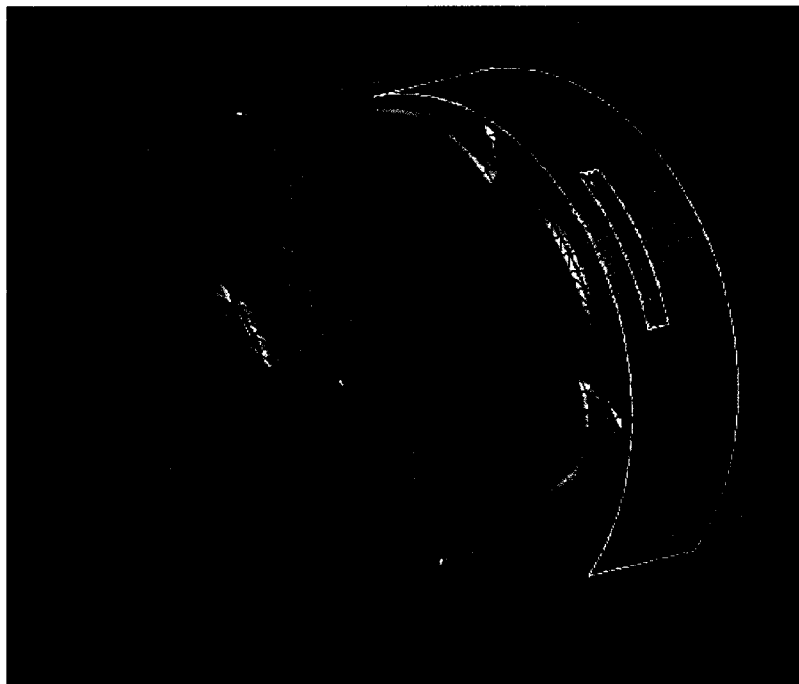
Figure 4.9: Swash plate bearing forces
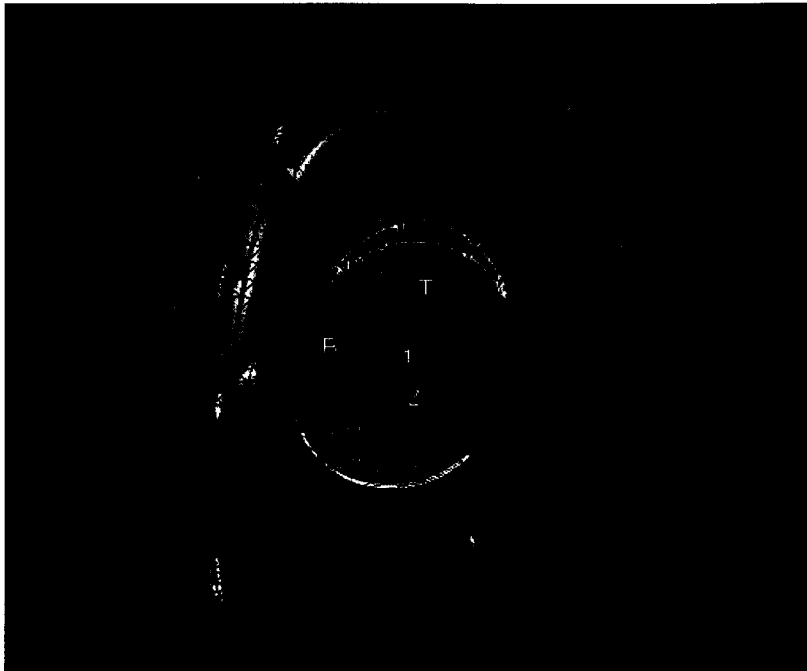
Figure 4.10: Swash plate constraint on center
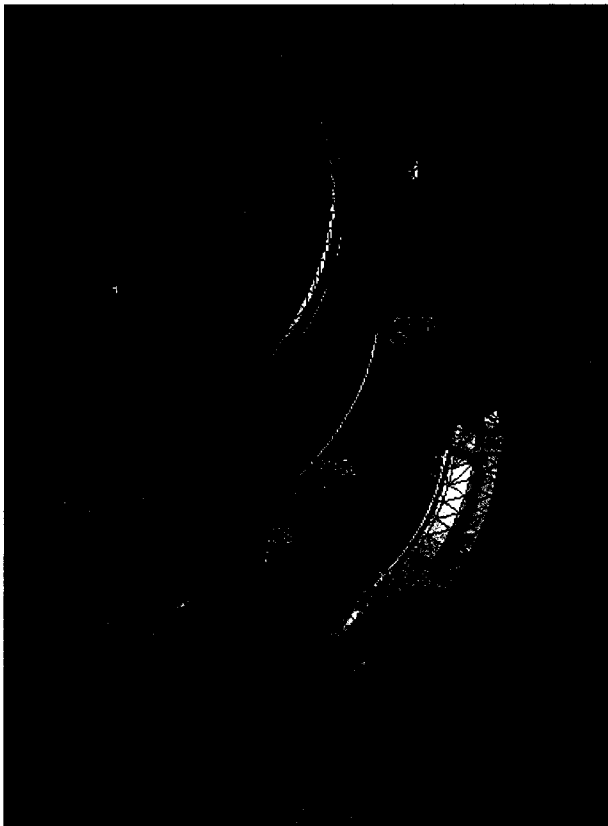
Figure 4.11: Constraints on edges

4.4 Important Governing Equations:

The maximum torque to be developed by the pump shaft to be transferred to fluid is calculated using

$$T = (\Delta P) D / 2ph_P \quad (1)$$

where T is the torque, (ΔP) is the maximum output pressure – 42MPa, at the maximum pump displacement, D (110 cc), and h_P (approximately 93%) is the pump volumetric efficiency when the pump speed is 2500 revolutions per minute, and the swash plate is at 23°. The force, F_r, at any spline section is calculated by dividing the torque by pitch radius, R_p at that spline (Figure 4.12). The arrows show the forces, F_r, calculated from

$$F_T = Torque / R_P \quad (2)$$
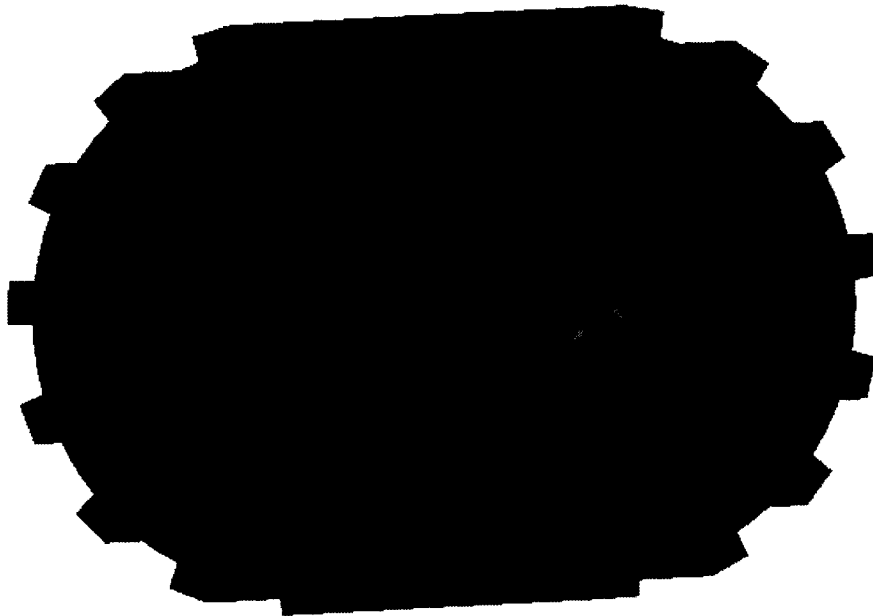
Figure 4.12: The splines of the shaft

4.5 Analysis:

The highest stress seen in any of the components was around 400MPa as found by the Von Mises method of calculation. The maximum displacement of the models was 0.1 mm. A Table of the results is shown below along with the method of calculation.

Table 4.1: NASTRAN results

Maximum	Barrel	Shaft	Swash plate	Piston
Von Mises (MPa)	66	239	298	924
Shear (MPa)	36	132	166	NA
Displacement (mm)	0.01	0.103	0.0295	NA
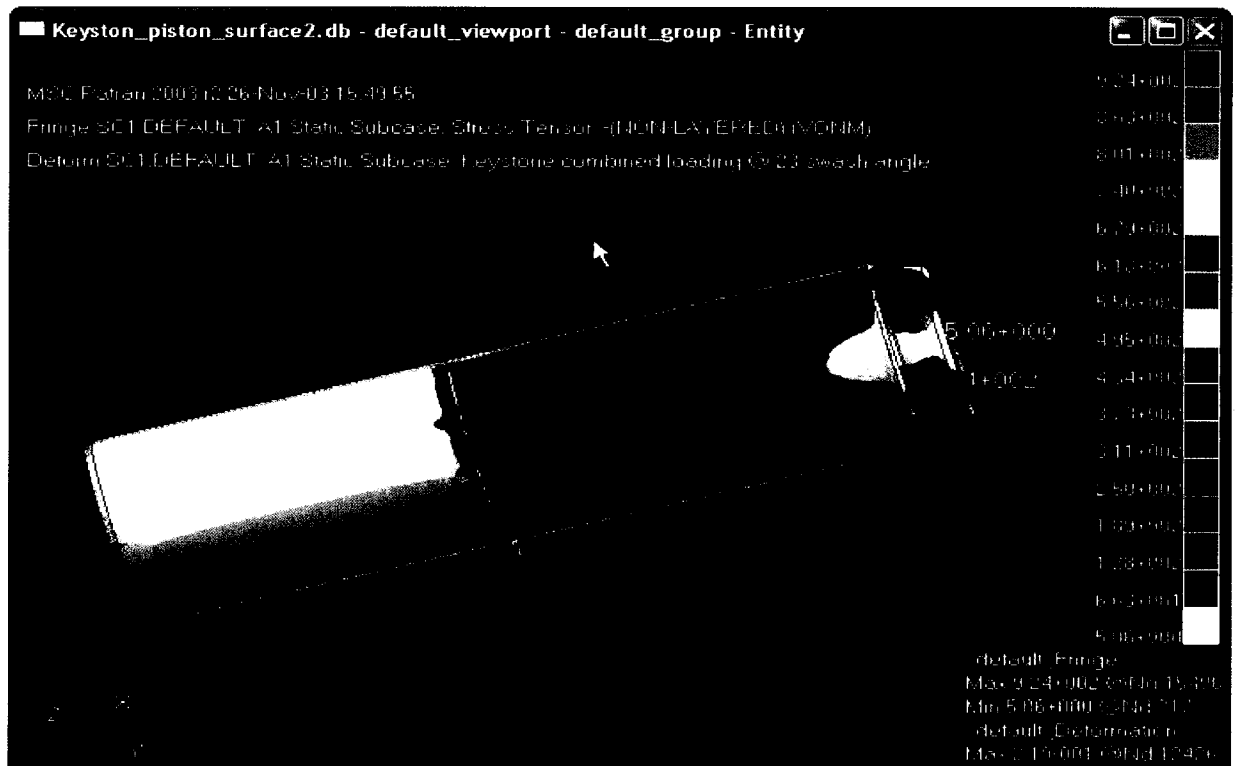
Figure 4.13: Piston combined load back: stresses & deformation (Ref. H. Zhang)

Figure 4.14: Piston combined load front: stresses & deformation (Ref. H. Zhang)

With the toques applied to the shaft, it showed the stress concentrations at the bottom on the teeth of the input shaft where they radius into the shaft column. The stresses at the barrel and output splines are about half the maximum stress, although displacement is the greatest at the barrel splines between the bearings. A Table of the results and Figures of the stress concentrations and displacements follow below.
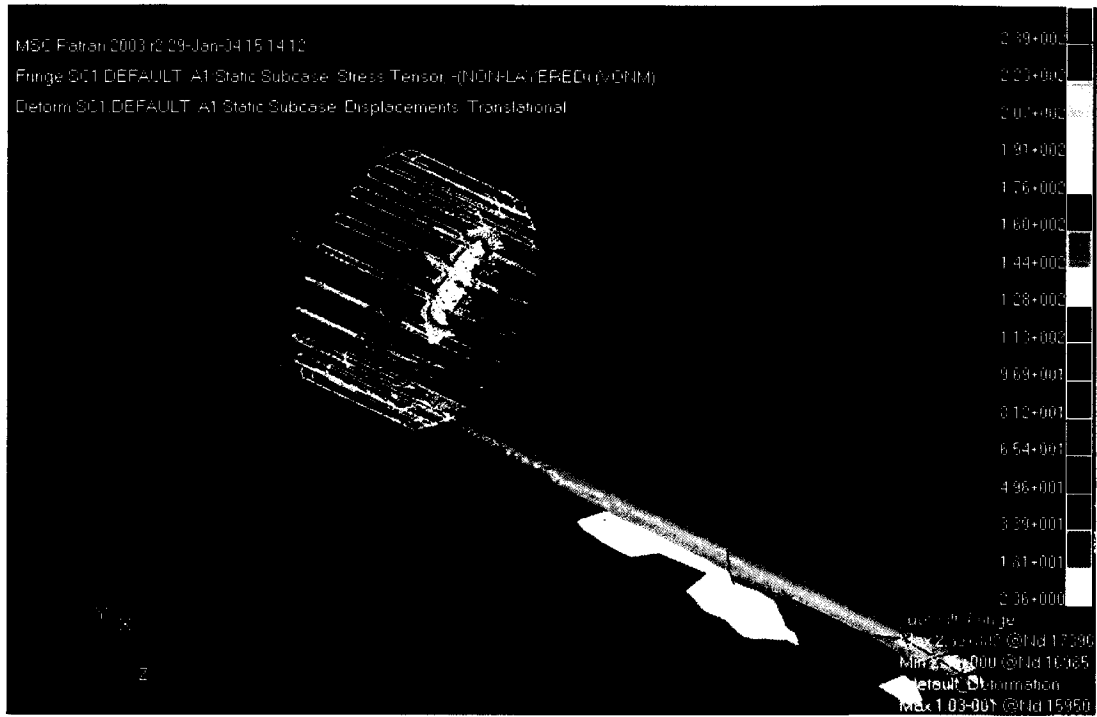
Figure 4.15: Shaft solid model dither on maximum Von Mises stress
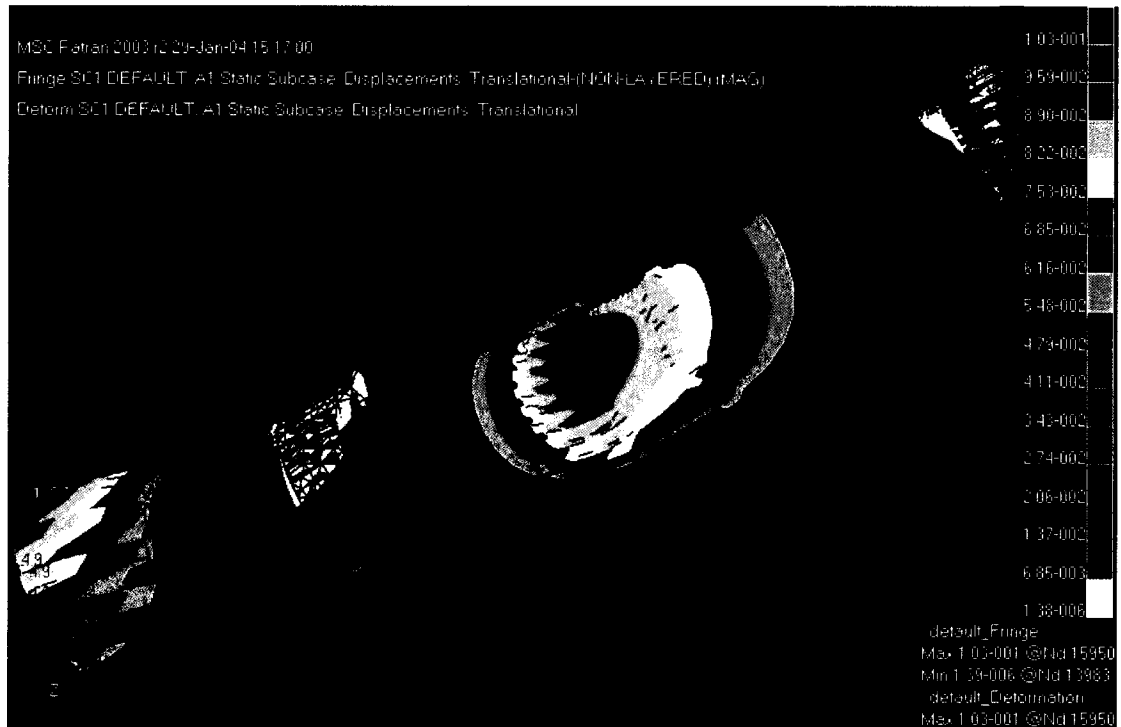
Figure 4.16: Shaft solid model dithered on maximum displacement

The stresses found on the barrel analyzed with the torque and forces applied were so low in comparison to the yield strength of the material and the displacements were so minimal that deeper analysis was not needed. Below is a Table of the results and pictures of the MSC.NASTRAN® results. The highest concentration of stress occurs below the lowest loaded piston bore. Although not the highest, stress also occurs along the splines as would be expected.

Table 4.2: NASTRAN barrel results

Maximum	Barrel
Von Mises (MPa)	66
Shear (MPa)	36
Displacement (mm)	0.01
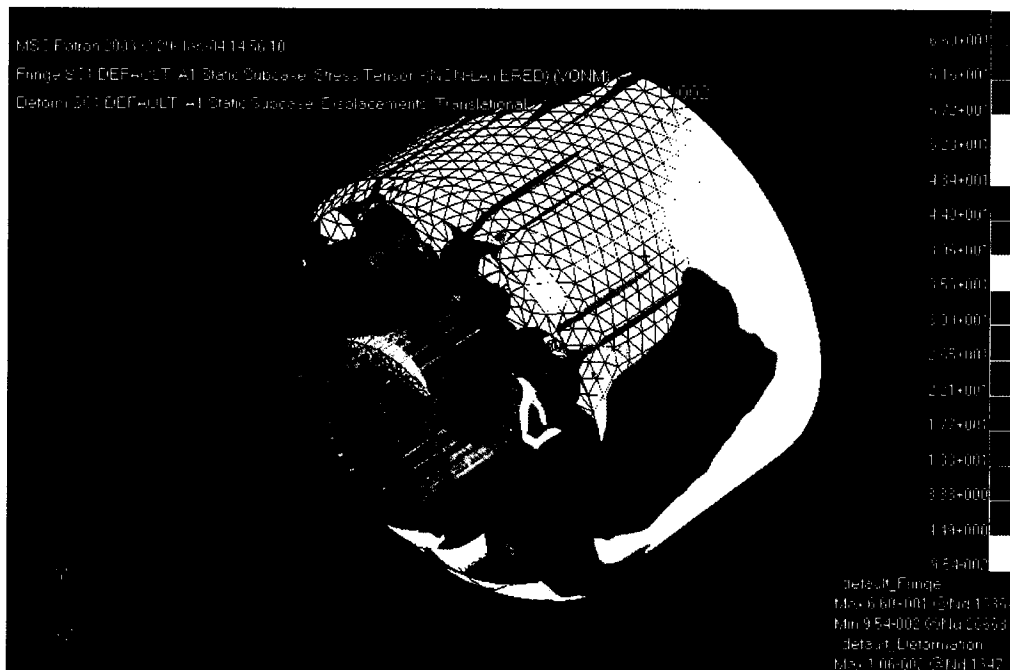
Figure 4.17: Solid model dither on maximum Von Mises stress
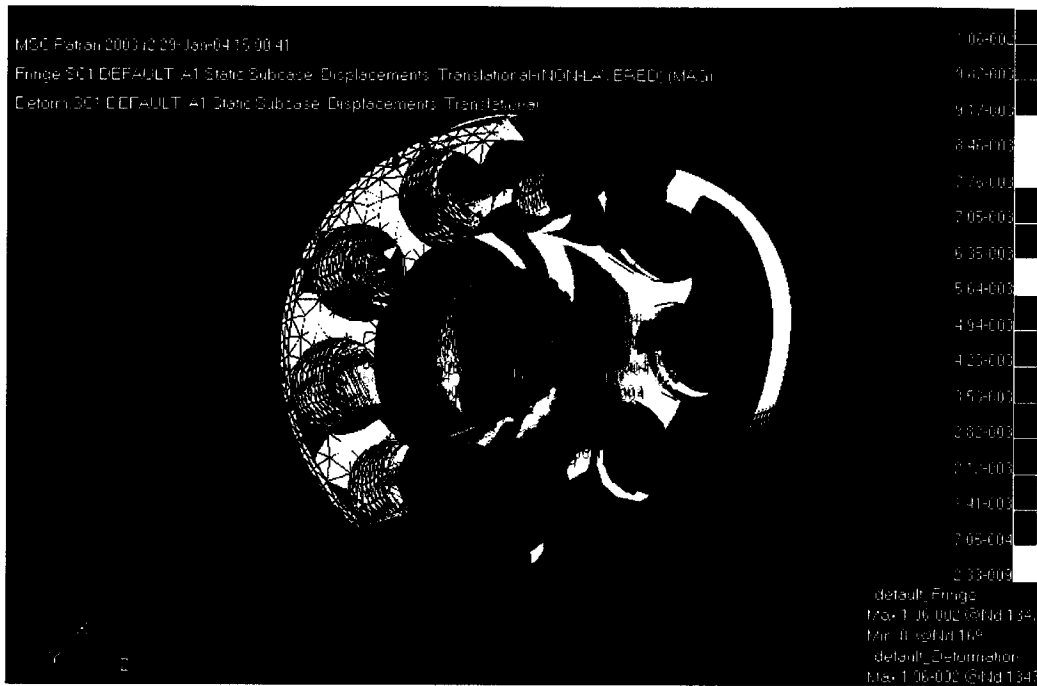
Figure 4.18: Solid model dithered on maximum displacement

The analysis on the swash plates were done to check the deflection of the plate and to see if it would deform enough to release the high-pressure ports. Therefore the stress analysis was not important. The Von Mises analysis was very high because of the constraints that were imposed around the center constraint. A Figure of the stress concentration is shown below. But the analysis of the deflection yielded very good results with a deflection of less than 0.1mm for both swash plate models before and after the modification by the designers. This is acceptable according to the Parker engineers.

Table 4.3: NASTRAN swash plate results

	Swash plate Model	Revised Swash plate Model
Displacement (mm)	.1	.08
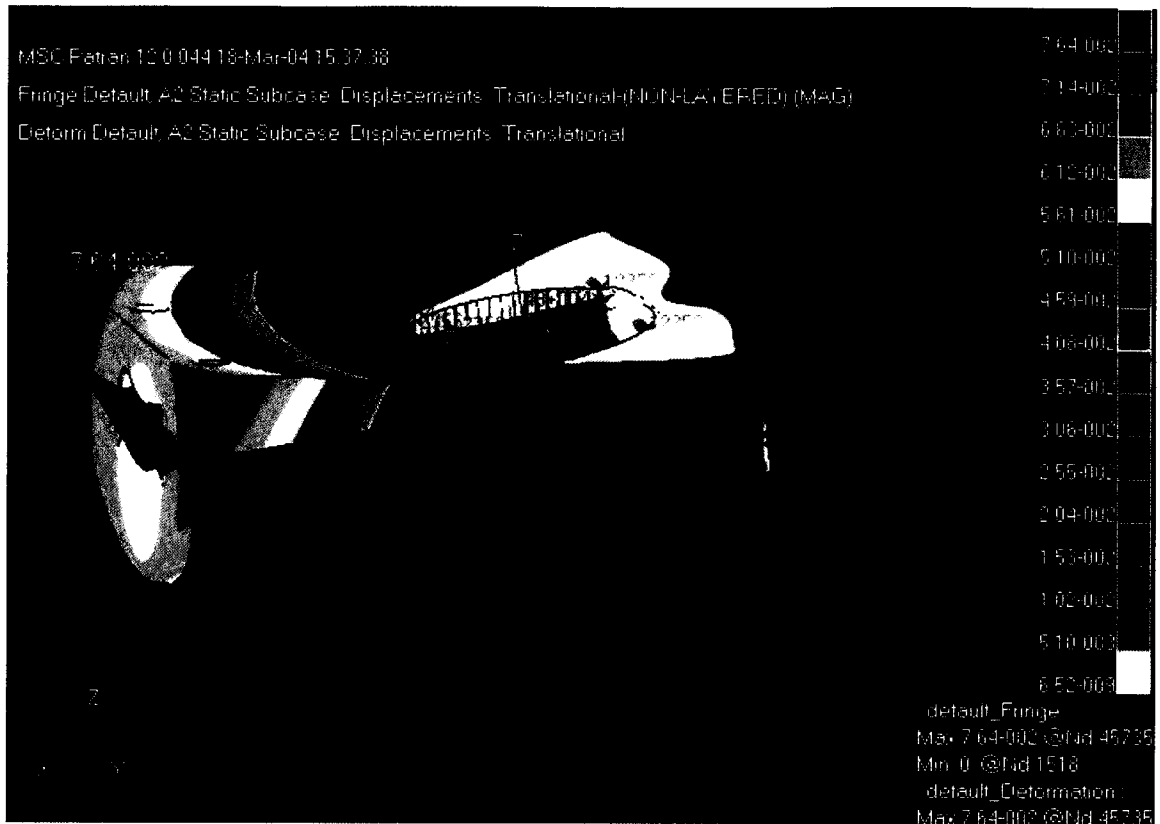
Figure 4.19: Revised swash plate dithered on displacement
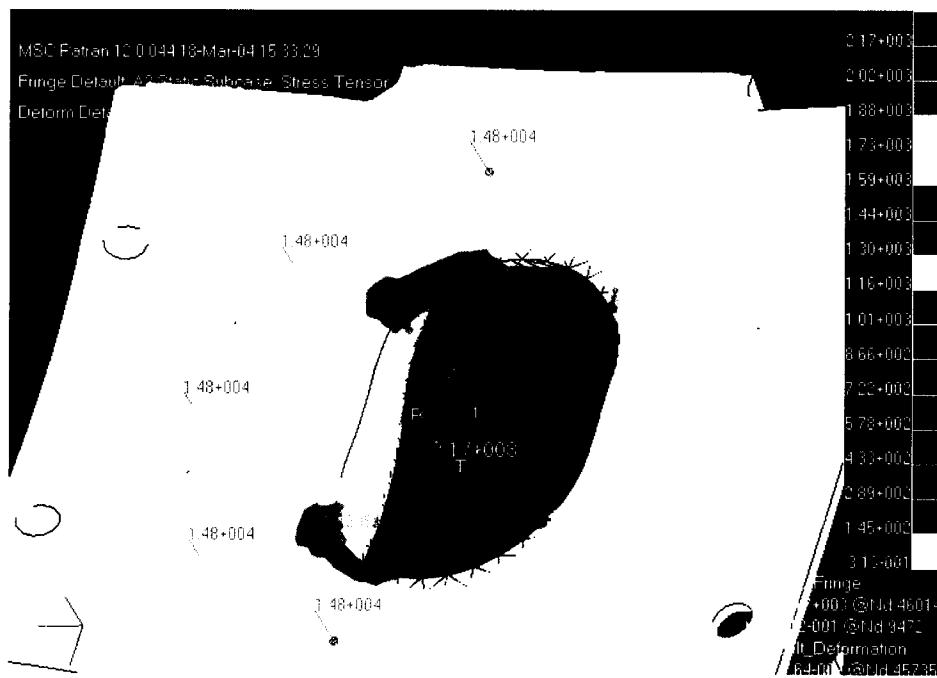
Figure 4.20: Revised swash plate showing stress concentrations

4.6 Conclusion:

The finite element analysis (FEA) was successful. The critical parts were studied carefully in order to insure that they can support the high loading upon motion found in Chapter 3 while running the rigid body simulation. The FEA revealed that the swash plate and the barrel are safe enough and can withhold the load upon operation. On the other hand, the shaft experienced high stress distribution and a deflection of 0.103mm that must be considered for further analysis. While for the piston, the stresses were found to be around 924MPa. This number is relatively high and further analysis should be done. Therefore, the swash plate and barrel were safe and piston and shaft were considered for the flex body analysis. This is done in Chapter 5; where the shaft and piston are added to the assembly as flex bodies. Furthermore, NASTRAN was used in order to generate the mnf files that are required for the input for ADAMS/View Flex body.

5   **FLEX BODY**

<u>5.1 Introduction:</u>

As discussed in the previous chapters, to study the dynamic behavior of forces/stresses during the pump operation and the consequent deformations of the critical components and their interactions with each other, we use ADAMS/View® with Flex Body Simulation. Such information cannot be obtained through rigid body simulation. This form of simulation is a very powerful tool in that the modeling approaches "the real world situation". It is noted in the Finite Element Analysis chapter (see Chapter 4), that of the critical components studied -- pistons, shaft, swash plate, and barrel, the stresses and deformations in barrel, and swash plate are negligible. Thus we can reasonably treat the barrel and the swash plate as rigid bodies. However pistons and shaft exhibit significantly larger deformations and deflections due to input pressure and consequent compressive and bending stresses. The results of the flex body simulation are helpful in optimizing the design such as modifying some dimensions and/or choosing the material of right strength in order to avoid failure of the component. The components to be modeled as flexible body are analyzed in MSC.NASTRAN® for mode shapes and frequencies (modal analysis). In such analysis, the components are meshed and material is specified, however no boundary conditions or loading conditions are input. The FEA thus conducted gives all possible mode shapes, and modal frequencies that can be visualized using MSC.PATRAN®. In MSC.PATRAN® 2004, the ADAMS interface is now available

in solutions 103, 111, and 112 for MSC.NASTRAN® 2004. This allows the creation of an mnf file for use with ADAMS in flexible body simulation. Therefore, we conducted modal analysis of the rigid body components – i.e., pistons and shafts, in order to create the flex bodies of the nine pistons and the shaft as mnf files, which have the mode shapes and are made of elements (from FEA). The flex body modeling is based on the mnf files, so what are the benefits of using mnf files and flex body simulation?

5.2 Benefits of Flex Body Simulation:

• Greatly simplifies the modeling of mechanisms containing flexible components

• Modal neutral-file format provides a self-contained data-transfer mechanism

• Helps assure that interaction between the component and the complete mechanical system is accurately modeled

• Allows fast simulations with no overhead from insignificant or inactive modes

• Reduces numerical integration effort by keeping inactive high-frequency response from adversely affecting solutions

• Helps the designer to interpret simulation results and gain insight into the model's characteristics

• Verifies flexible-body data and modal content, and let the designer investigate interaction with control systems

With the help of ADAMS/Flex, one can incorporate the components that are created in FEA within the ADAMS/View simulations to see how the overall system performance is affected by having these flexible bodies within the

complete mechanism design. It also lets one use the results of the simulation to provide accurate loads and flexible-structure displacement data to FEA for studying the effects of motion and forces on individual mechanism components. By coupling motion simulation and FEA in this way, this can help one to improve the accuracy of the full-system simulation and brings it closer to true system-level design and engineering.

• View FE mesh within the full system assembly to manage the flexible body's attachments and attributes

• Draw, animate, enable, or disable a component's modes

• Automatically disable component modes contributing small amounts of strain energy

• Scale deformation to enhance visual feedback

• Recalculate inertia invariants

• Represent deformation in color contours, with complete control over deformation reference

• Replace flexible-body graphics, if needed, with outline sketches

• Animate component modes, system modes, and simulation results

• Use the powerful plotting capabilities to study the results of your simulation.

5.3 Objective:

Our objective is to build a flexible model that is as close as possible to the true system investigated. The model investigated is a concept pump with a swash plate angle of 23°, the shaft rotational speed of 2500 rev/min, and the

output pressure profiles provided by Parker design engineers. Different cases were run, first after running the rigid body full simulation some modifications were made in order to begin modeling flex body, fist a model with two diametrically opposite flexible pistons was built. The next step was adding the flexible shaft to the model and running the simulation. Then after that we went on and added the whole nine flexible pistons with the flexible shaft and run the simulation, the full flexible body simulation took around three hours to be done.

Figure 5.1: The flex body piston pump prototype

5.4 Procedure:

In order to run the full flex body simulation and get the results, the rigid body model was modified by the introduction of two diametrically opposite flexible

pistons as a first step. Then the nine flex pistons and shaft were added to the model with the required modifications like for example assigning the executable solver as C++ instead of FORTRAN which can not handle the flex body with the location of the markers being modified. In other terms, the topology of the model has changed so that the markers are no longer connected in a way that is compatible with the ADAMS/Solver (FORTRAN). Therefore, C++ was used instead. To be mentioned that the flexible parts being as mnf files, were provided from the MSC.NASTRAN® analysis on the piston and shaft. Having these mnf files and connecting them with the different adjacent parts, the full flex body simulation was performed with an input pressure of 42MPa.

When the flex body was modeled some modifications were made, among them, once the flex piston is imported to ADAMS/View® the different markers a linked to this piston had to be reviewed and a Center of Gravity marker had to be created for every flex body. This CG marker was used for the location of the applied force due to pressure and the change in the angle that is connected to the rotation of the pump. Moreover, the CG marker was also used to connect the flexible body to the corresponding adjacent part. Notice that the different types of joints that were used for rigid body remained the same but the connectivity with the flexible bodies (i.e. the corresponding markers) had to be reviewed and connected to the CG created again. Then the same procedure as the rigid body was used, the pressure of 42MPa was input through the AKIMA function as a variable force varying with the angle of rotation, where each piston lagged the previous piston by 40°. The next step was to introduce friction force between the

slippers and the retainer plate and the pistons and the bushings. Therefore, the static and dynamic friction factors were changed for each contact force between the slippers and retainer plate. The μ_{static} =0.2 and $\mu_{dynamic}$ =0.05. Friction was modeled as dry. After doing so and activating all the forces from pressure profile to friction to contact forces we ran the simulation. Thus the ADAMS models were built and simulated per the following matrix in Table 5.1, showing the number of simulations runs for some key parametric changes. The discussion below highlights analysis of results for output pressure of 42MPa.

Table 5.1: Matrix of simulation runs

Run No.	Output Pressure MPa	Shaft Speed RPM	Swash Plate Angle Degrees	Flexible body used
1	42	2500	23	Rigid
2	42	2500	23	2-pistons
3	42	2500	23	9-pistons
4	42	2500	23	9-pistons &shaft

<u>5.5 ADAMS Simulation Results and Analysis:</u>

In analyzing the full assembly as a flex body and after getting a feedback from the Finite Element analysis, we were concerned about the shaft and the pistons in terms of stress distribution. Therefore, the barrel and swash plate were considered as rigid and the shaft and piston as flex based on previous studies (Finite Element Analysis, Chapter 4).

We will begin with the input force, which is 12500N calculated as follows:

$$F_{DK} = A_p \, (P_K)$$

$$= (298 \ast 10^{-6} \ m^2) \ast (42 \ast 10^6 \ N/m^2)$$

= 12516 N.

Note that the input is a force that acts at the center of gravity of the piston and this force is the reaction of the pressure input of 42MPa. MSC.ADAMS® does not accept pressure; therefore the pressure was transformed into a moving force by multiplying it with the desired area.

Figure 5.2 shows the pressure forces as an input for a randomly chosen piston 2, 3 and 4. They are step forces acting only for a period of time and they are shifted by a 40° angle. Their maximum absolute value is 12500N.
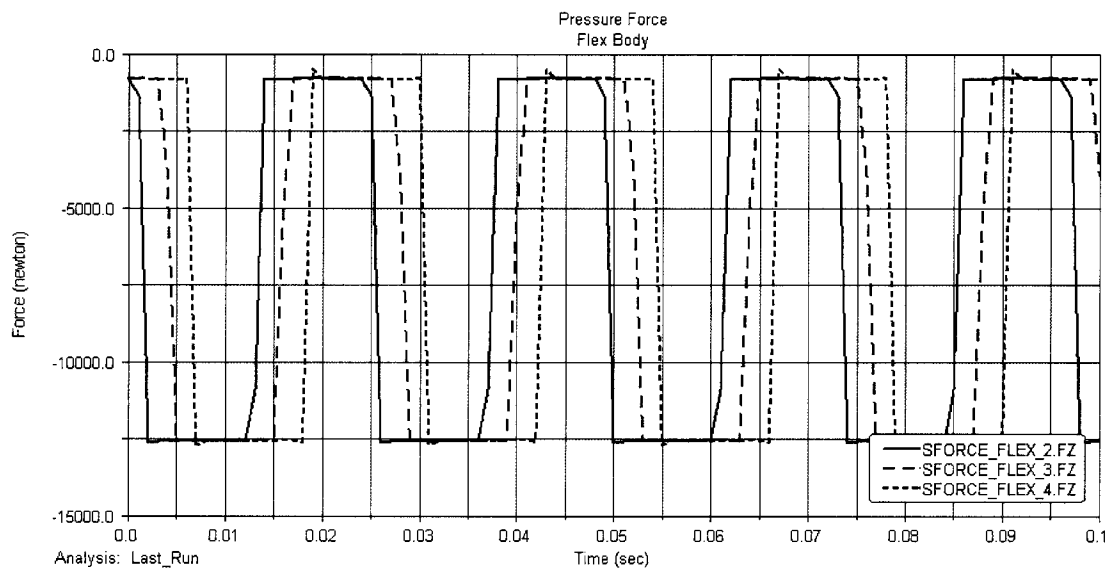
Figure 5.2: Pressure force for flex body simulation

Plotting the forces with respect to the rotation angle shows us the pressure distribution at different locations. Figure 5.3 below illustrate this idea for rigid body and flex body simulations respectively.
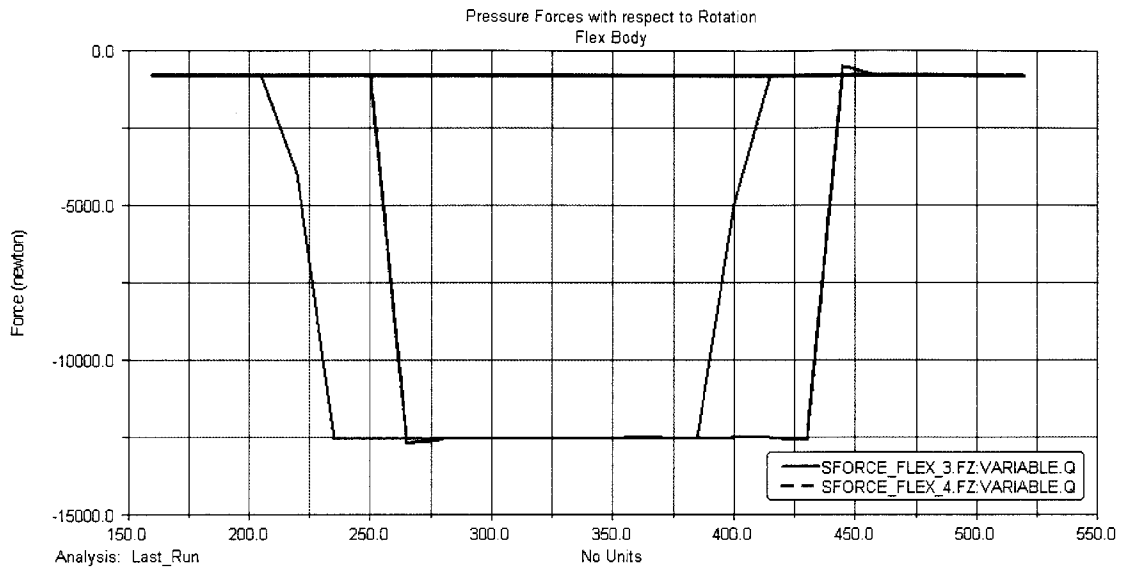
Figure 5.3: The pressure profile with respect to the angle of rotation for flex body

Also note that force components on piston 3 and 4 are chosen randomly. It could have been any of the nine pressure forces.

The angle mapping for each piston locates its position with respect to the rotation of the shaft (rpm) is shown in Figure 5.4 below. Each angle covers 360° per one revolution of the pump. And it is associated to a piston that ensures the location of this piston at different time. Notice the phase difference between two consecutive angles is 40°.

The angle mapping is shown below in Figure 5.4 with three randomly chosen variables:
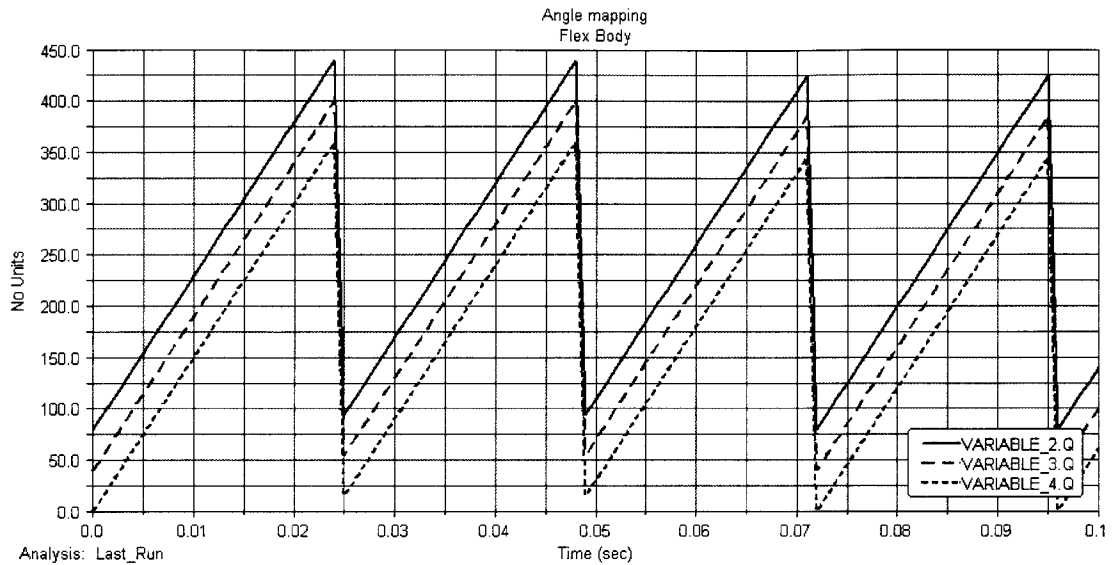
Figure 5.4: The angle mapping for the flex body simulation

Notice that there is no difference between the rigid (Figure 3.5, Chapter 3) and flex body graphs as expected because the state variable connecting the piston location or angle and the rotation is an input entity for the design and should be the same.

Forces between the pistons and the barrel are also investigated because they are important for the design and give ideas about what is happening in the interaction between the piston and the barrel (or sleeves).

For the Flexible body simulation, we have the following:
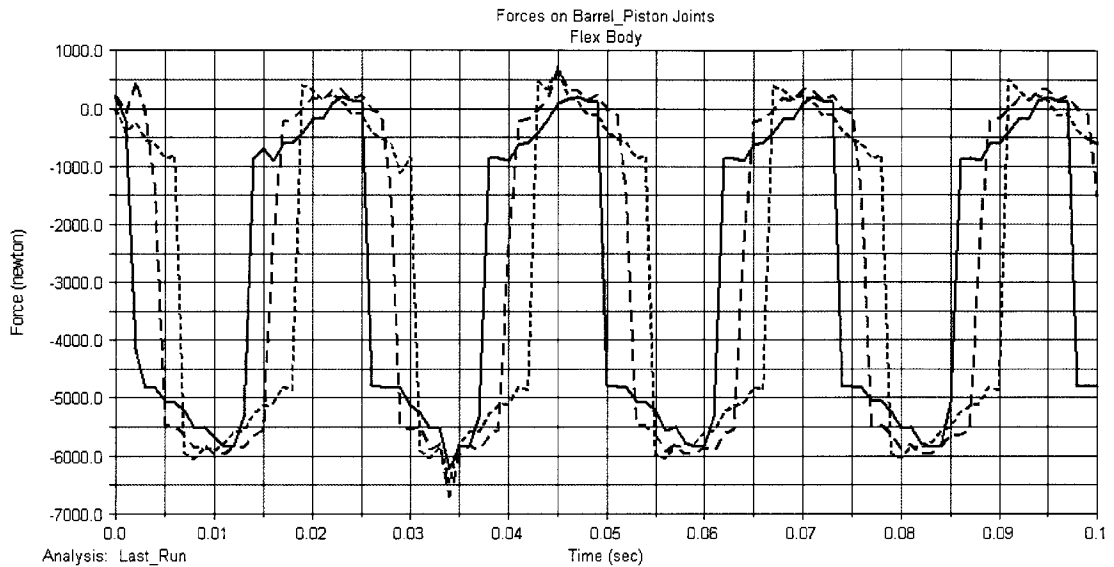
Figure 5.5: Forces on the barrel piston-sleeve joint in the Y-direction for flex body simulation

If we compare the rigid body (Figure 3.6, Chapter 3) and the flex body graphs we notice that the two graphs are identical. We can see that we have the same maximum value of 6000N over one revolution. But there is a slight difference in the peaks where the flex body curves seems that are more distorted while the rigid body the peaks are more rounded and smooth. These findings are important for the designers to see if the bushing design is safe or not in terms of material picking and treatment and dimensions (thickness, length, clearance, etc).

Another parameter investigated as a finding that is helpful for the designers is the forces between the slippers and the pistons. These forces are needed to be found to insure that the slippers are not subjected to high loads that may cause failure or fatigue, especially in the change of shape from the ball round part to the flat part where the stress concentration will take place.

The Flexible body simulation reveals the following results for the forces between the pistons and slippers shown in Figure 5.6:

Forces On Piston_Slipper joints
Flex Body
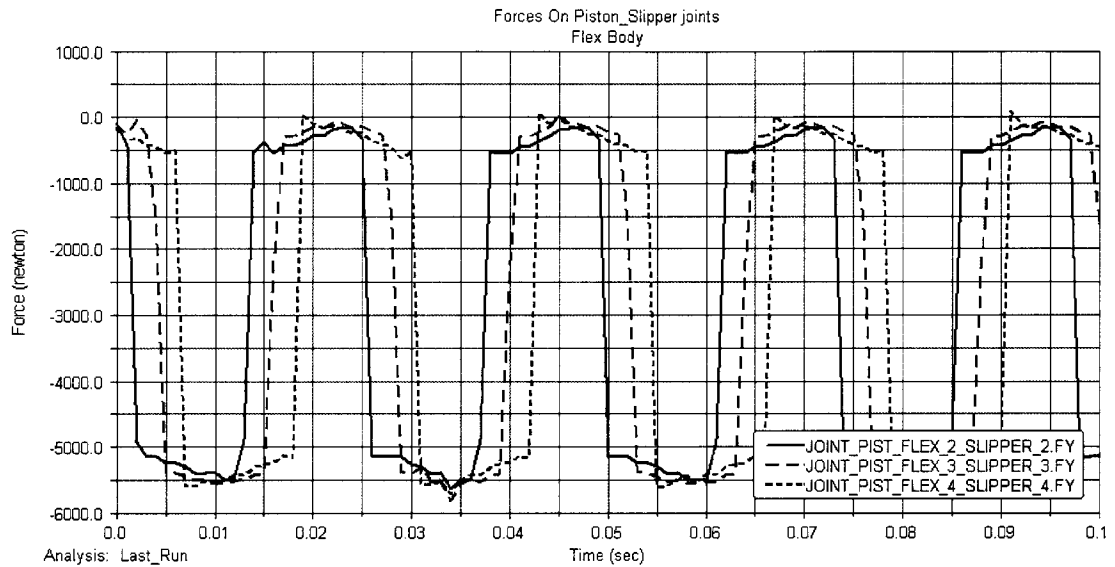
Figure 5.6: Forces on the piston slipper joint in the Y-direction for flex body simulation

Similarly, the forces between the swash and slipper interface were found. These values are found to be equal and opposite of the forces on the slipper piston interface. The maximum value is of 5500N. This is shown in Figure 5.7:
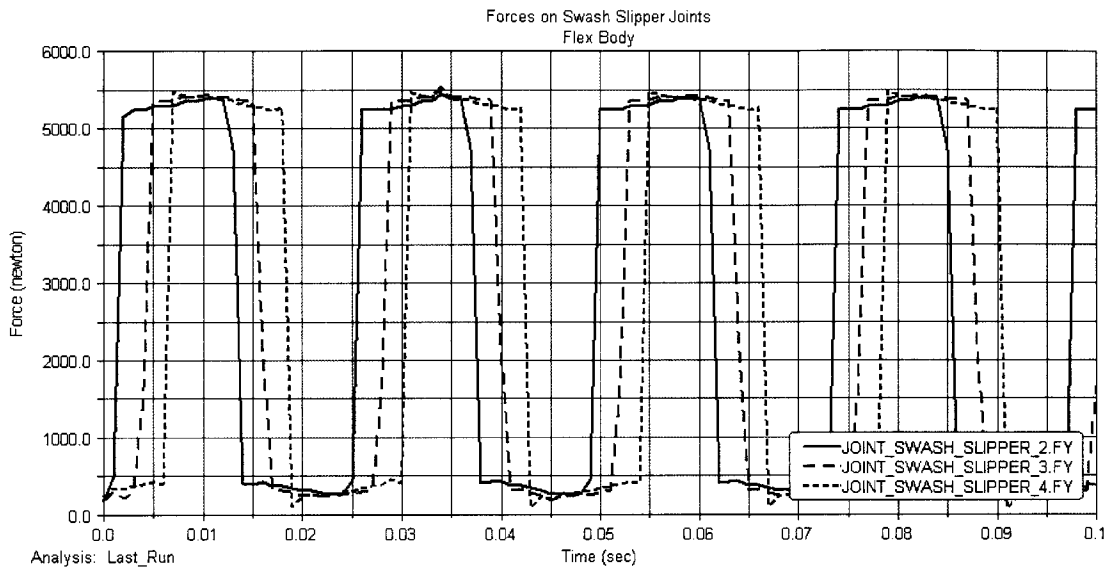
Figure 5.7: Forces on the swash plate slipper joint in the Y-direction for flex body simulation

The same values of 5500N are found for the forces between the swash plate and the slipper retainers for the rigid and flex body simulation that mean that the flex body did not affect the swash-slipper interface.

In order to make sure that the shaft design is safe, the forces on the shaft ground joint were one of the important findings, because again the shaft is a flex body and its behavior in dynamic motion must be know to avoid errors.

The Flexible body simulation reveals the following:
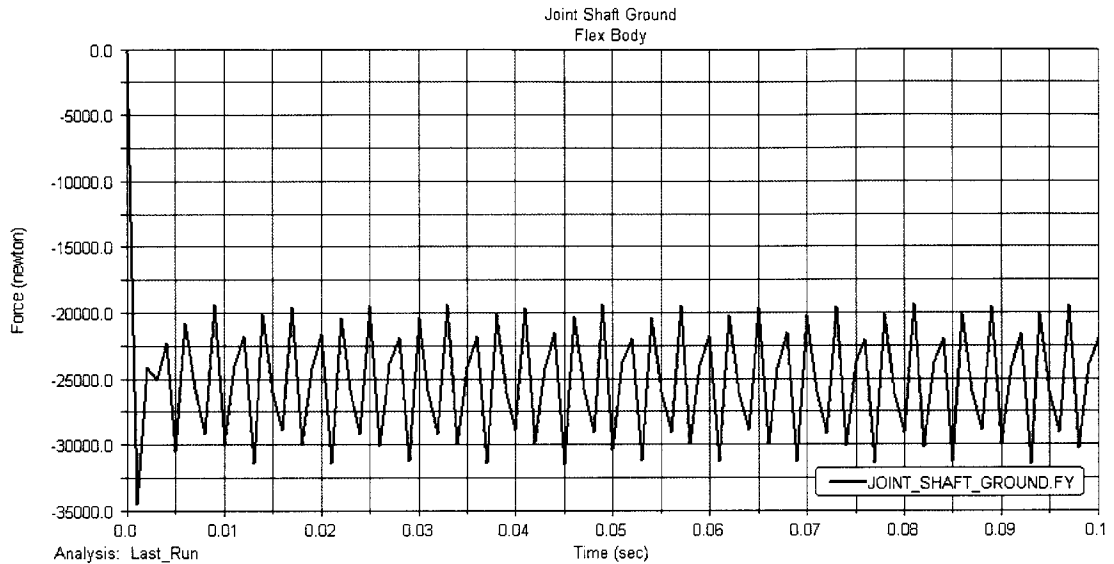
Figure 5.8: Forces on the shaft ground joint in the Y-direction for flex body simulation

Looking at Figure 5.8, notice that the average value of the force on the joint between the shaft and ground in the y direction for the flex body simulation is -25015.12N and the maximum and minimum values are respectively -20120.68N and -34458.39N.

To be mentioned that the difference between the values from the rigid body simulation and the flex body simulation are very minimal. For example, the difference between the two average values is around 0.93%. While the maximum and minimum values show a higher difference that is 13.9% and 22% respectively. This result is as expected because the flexible shaft is allowed to deform while rotating and which means that the joint will be subjected to higher forces to compensate for the deformation. This is seen in the difference of the numbers shown above. Investigating the graphs more carefully, we notice that the minimal value of -34458N is just at the beginning and it is random, it is not a repetitive pattern, therefore, we can read a minimum value of 31000N that is

repeated in each cycle. So the spontaneous high value at the beginning can be interpreted as a result of software solver weakness.

The deflection of the piston for the flexible body simulation in the X-direction is shown in Figure 5.9 below:

MEA_PT2PT_10
Deflection in the X-direction
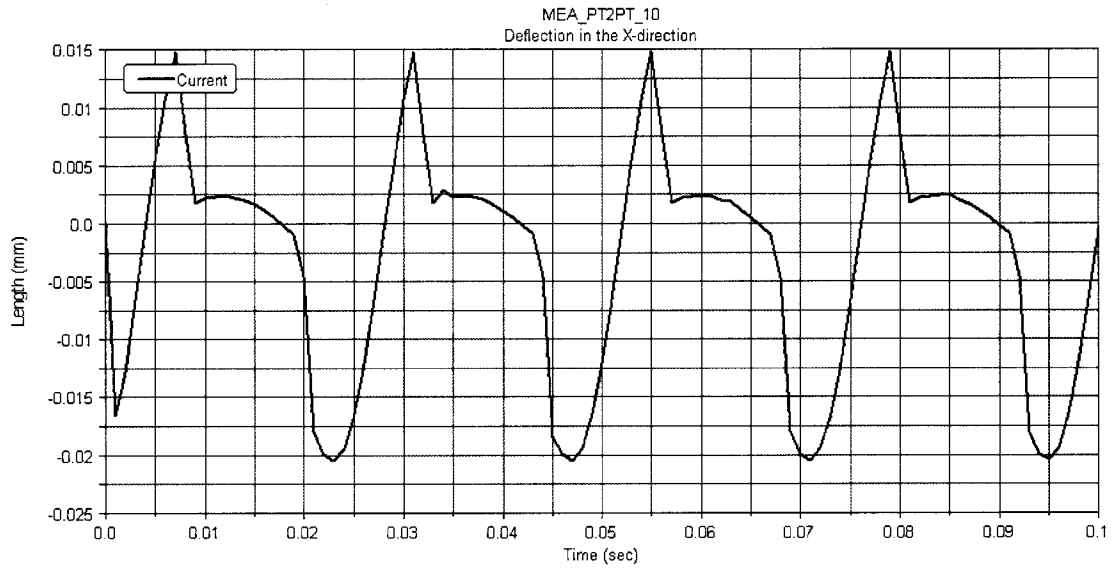
Figure 5.9: The deflection of the center of mass of the flex piston

Combining the X and Y components of the deflection of the center of mass of the flexible piston is shown in Figure 5.10 below:
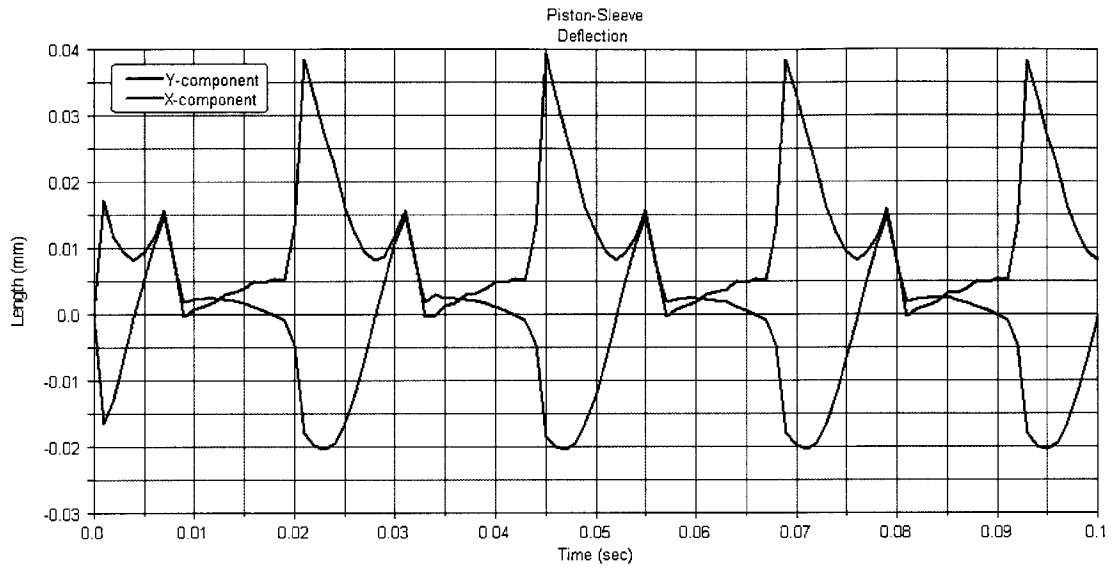
Figure 5.10: X and Y components of the deflection of the center of mass of the flex piston

We notice that the maximum deflection of the piston is around 0.02mm. This deflection is the measure of the distance between the center of mass of the flex piston and the center of mass of the sleeve. Originally at time zero, both centers of mass were coincident, and as the simulation goes on, we can see the piston deflected from its original position upon the action of the input pressure.

Another important finding is the center of mass position of the shaft. This is of interest for us because in this way we can predict the distance that the center of mass moved from the original rest condition and can calculate the worst deflection upon dynamic motion of the full assembly.
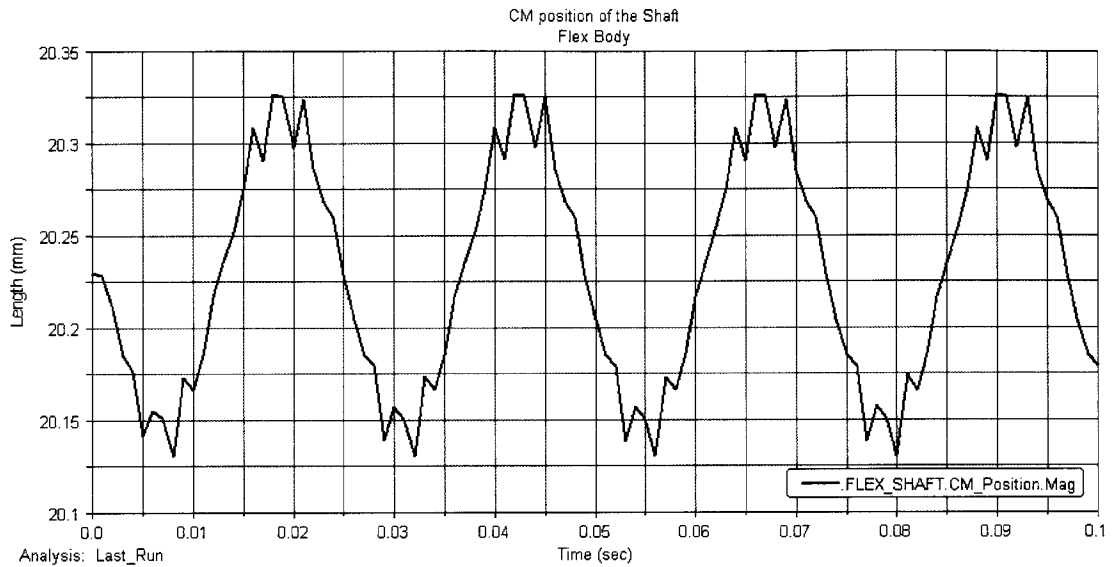
Figure 5.11: The center of mass of the shaft for flex body simulation

Notice that the center of mass for the shaft being as a rigid body (Figure 3.10, Chapter 3) is constant and does not change, which is expected because the shaft is not supposed to deflect. Its value is 20.08mm. While the center of mass for the shaft being as flexible, we can see the change in the position between a maximum value of 20.3265mm and a minimum value of 20.1302mm, and an initial value of 20.23mm. The highest deflection is δ= 0.099mm, which is the difference between the initial and minimum value.

Now, as done in Chapter 3 for the rigid body, we investigate the angular kinetic energy of the shaft for the flex body simulation and we will validate the results by using theoretical calculation.

The kinetic energy for the shaft using it as flexible body is shown in Figure 5.12:
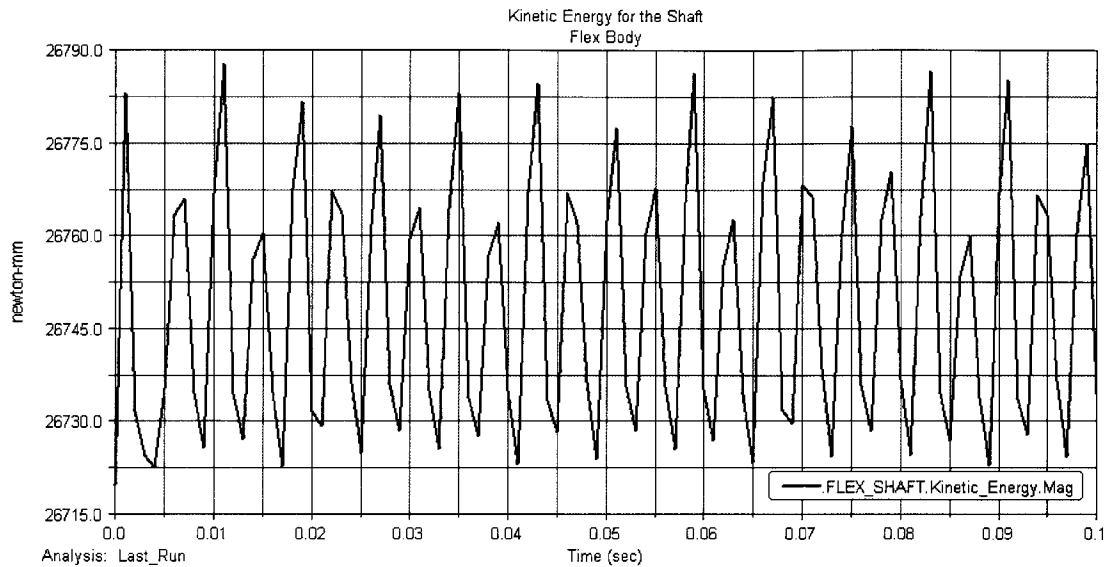
Figure 5.12: Kinetic energy for the shaft flex body simulation

The angular kinetic energy of the shaft is validated by using hand calculation. The mass of the shaft is m_{shaft}= 3.4651566 Kg and the radius is about R = 15mm with the angular velocity of 2500rev/min, using the following we get:

$$KE = \frac{1}{2}(m)(R\omega)^2$$

$$KE = \frac{1}{2}(3.4651566kg)\left(\frac{(15\times10^{-3}m)\times 2500\times 2\pi}{60\sec}\right)^2\left(\frac{1000mm}{1m}\right)$$

= 26718.535N.mm

Notice that the angular kinetic energy for the shaft with the flexible shaft is between the two values **26719.75N.mm** and **26783.20N.mm**. Comparing these values with the theoretical calculation above we see that the error is around 0.24% for the flexible body simulation.

Similarly, we investigate the angular kinetic energy of one of the pistons in the flex body simulation and we will validate the results by using theoretical calculation.

The kinetic energy for piston 2 using flex body simulation is shown in Figure 5.13 below:
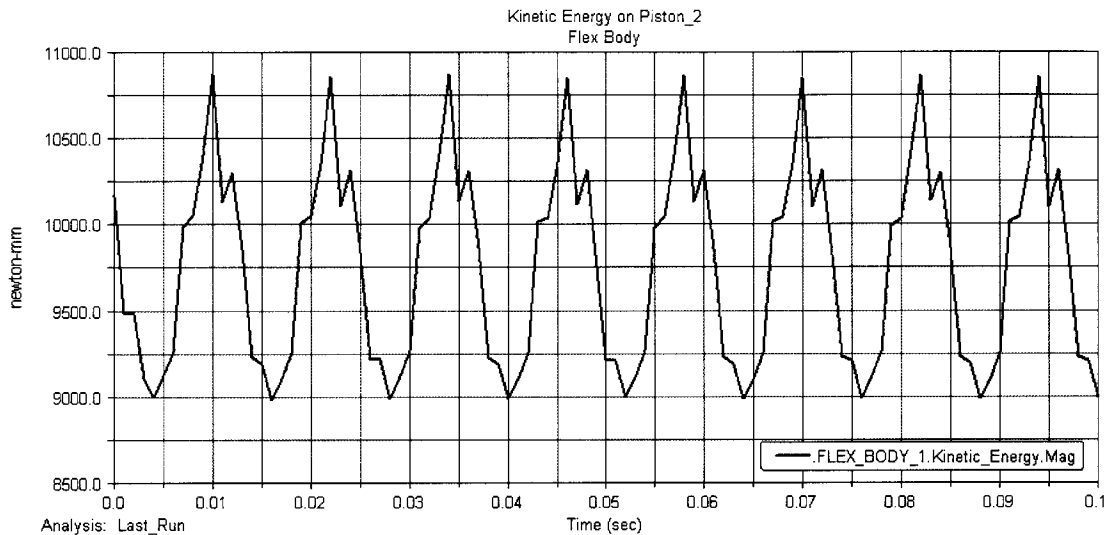
Figure 5.13: Kinetic energy for piston 2 flex body simulation

The theoretical calculation of the angular kinetic energy of the piston is validated by using hand calculation. The mass of the piston is $m_{piston}=$ 0.12801098 Kg and the radius is about R = 46mm with the angular velocity of 2500rev/min, using the following we get:

$$KE = \frac{1}{2}(m)(R\omega)^2$$

$$KE = \frac{1}{2}(0.12801098kg)\left(\frac{(46\times10^{-3}m)\times2500\times2\pi}{60\sec}\right)^2\left(\frac{1000mm}{1m}\right)$$

= 9282.61N.mm

Notice that the kinetic energy of the flexible piston has an average value of **9763.60N.mm**. This value is oscillating between 9000N.mm and 10868N.mm as expected because the piston is moving back and forth and undergoing a periodic motion. Comparing these values with the theoretical calculation above we see

70

that the error is around 4.9% for the flexible body simulation. This result is close to the theoretical calculation. Also, comparing Figure 5.13 with Figure 3.12 (Chapter 3, Rigid Body), we see that both have the same pattern, while the flexible body has sharp ends and the rigid body is perfectly smooth.

The torque between the retraction plate and the slipper is found to be as follows in Figure 5.14:
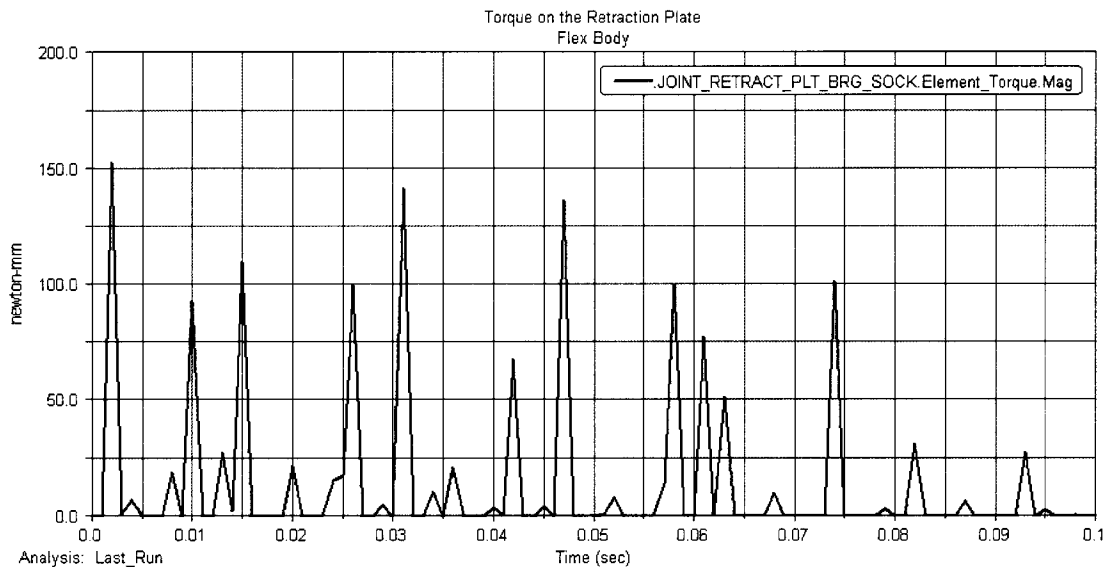
Figure5.14: Torque between the retraction plate and the slipper

The maximum value is around 155N.mm, which is a relatively low value of the torque and does not affect either component.

The contact forces between the pistons and sleeves are shown in Figure 5.15 below:
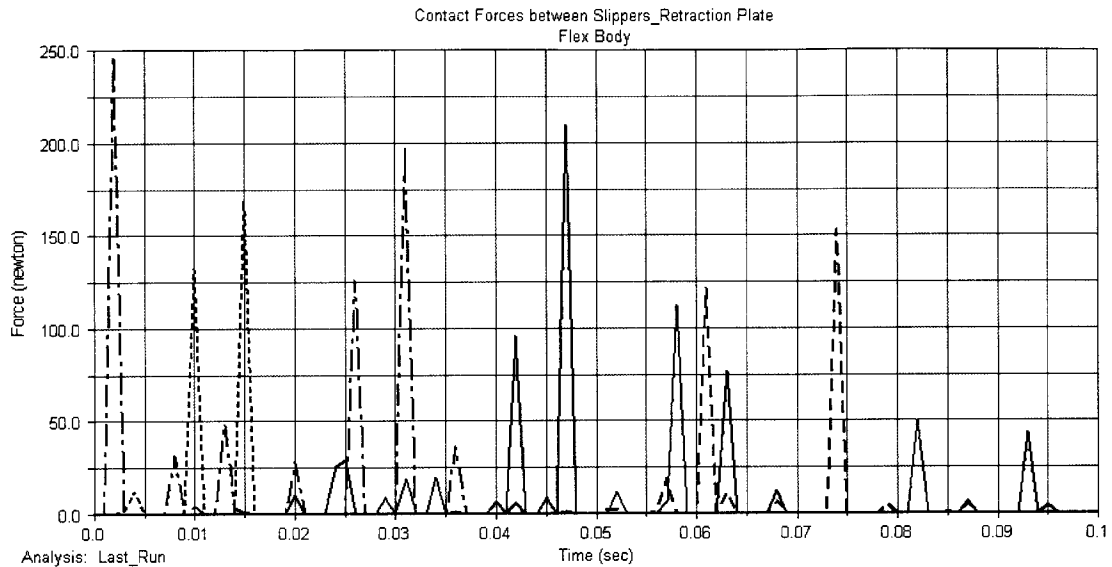
Figure 5.15: contact forces between the slippers and retraction plate for Flex Body simulation

Notice that the contact forces between the slippers and the retraction plate are in a reasonable range, where the highest value is around 250N. To be mentioned also that the flex body here does not affect the value of the contact forces between the slippers and retraction plate dramatically. Running the rigid body simulation with the same set up gives values of around 400N as shown in Figure 3.13 (Chapter 3).

Then, the contact forces between the pistons and the sleeves were found for the rigid body only. Contact forces were not assigned for the flex body simulation because of the technique used in building flex body components. In other words, a flex body is not made from a shell and a part so to be able to assign contact to it. Ways can be done to add contact forces to a flex body, but the flex piston must be modified in MSC.NASTRAN® prior to the generation of mnf file. This option was not available to us, so we added translational joints between the pistons and the sleeves.

Notice that the contact force has a maximum value of 5327.24N and a minimum value of -1499.98N. These values are not in a critical range keeping in mind that the contact that we modeled is a dry contact with no lubrication that minimizes the contact force and friction.

The Flex Body simulation reveals the moment on the swash plate, which is plotted in Figure 5.16:
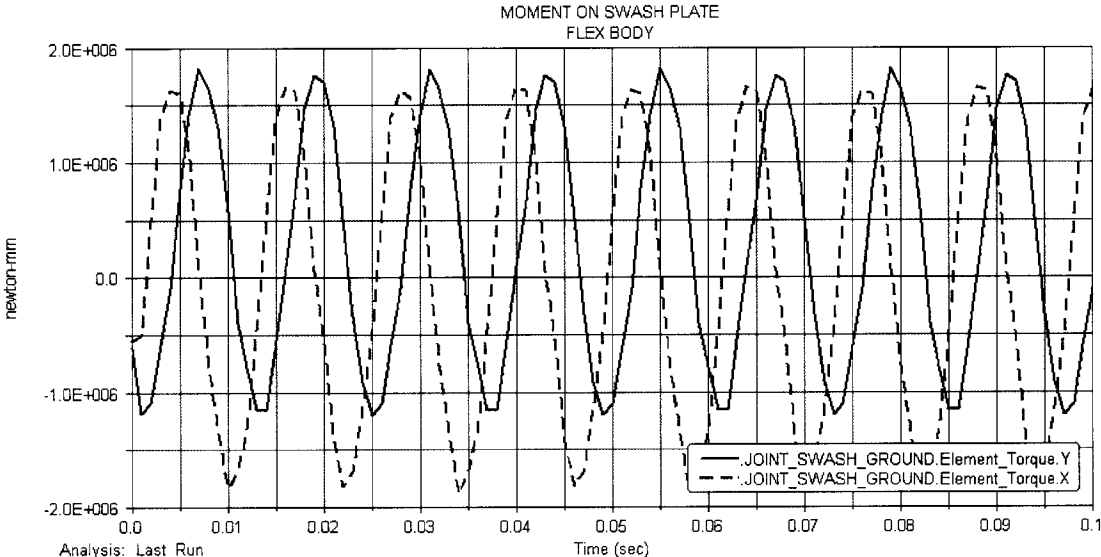
Figure 5.16: The moment on the swash plate for flex body simulation
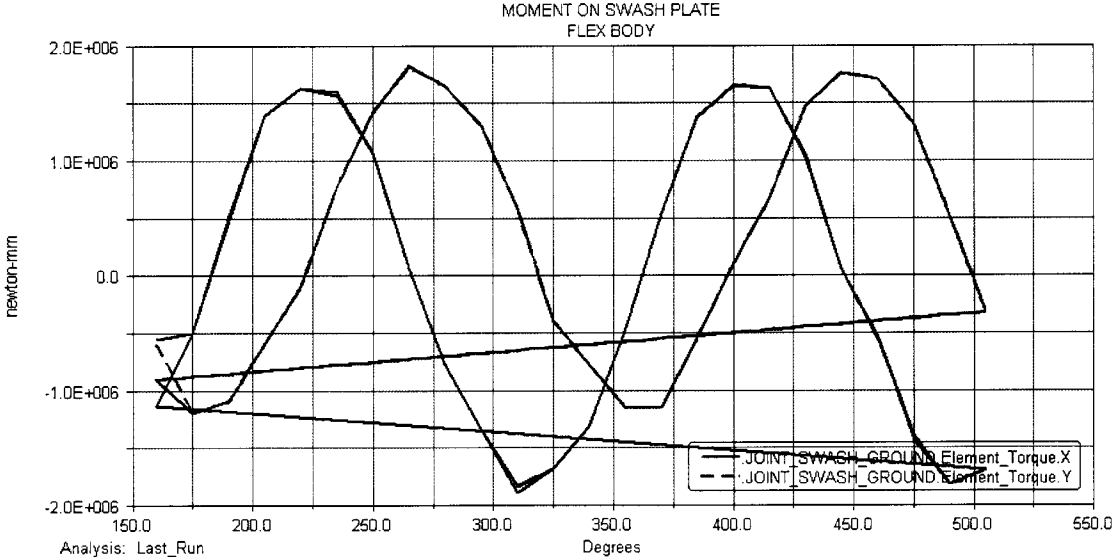
Figure 5.17: The moment on the swash plate for flex body simulation with respect to the angle of rotation

Investigating the results more closely, we get the maximum and minimum values of the torque on the swash plate in the x-direction for the rigid and flex body simulation to be tabulated in Table 5.2 as follows:

Table 5.2: Moment on the swash plate

Simulation	Rigid body		Flex body	
Value	Max	Min	Max	Min
T_x (Nmm)	1.721×10^6	-1.804×10^6	1.658×10^6	-1.890×10^6
T_y (Nmm)	1.822×10^6	-1.208×10^6	1.823×10^6	-1.195×10^6

Comparing the values from Table 5.2 above, we see that the difference between the maximum values for the rigid and flex body simulations is that the rigid body moment in the x-direction is 3.8% higher than the flex body simulation. The purpose of calculating moments on swash plate is to estimate the forces on the bearing that is located between the swash plate and the casing of the pump and study the severity of the forces exerted. The comparison of moments for rigid and flex body are tabulated in Table 5.3:

Table 5.3: Percentage difference between rigid and flex simulations

	Difference in maximum	Difference in minimum
T_x	3.80%	4.76%
T_y	0.18%	1.08%

5.6 Durability Analysis:

The deflected shape of the flexible body simulation is shown in the Figure below. Note the change in color is where the stress is relatively higher. To be

mentioned that a scale factor of 25 was taken in order to magnify the deflection, i.e., the deflections shown below are 25 times magnified from the true scale.
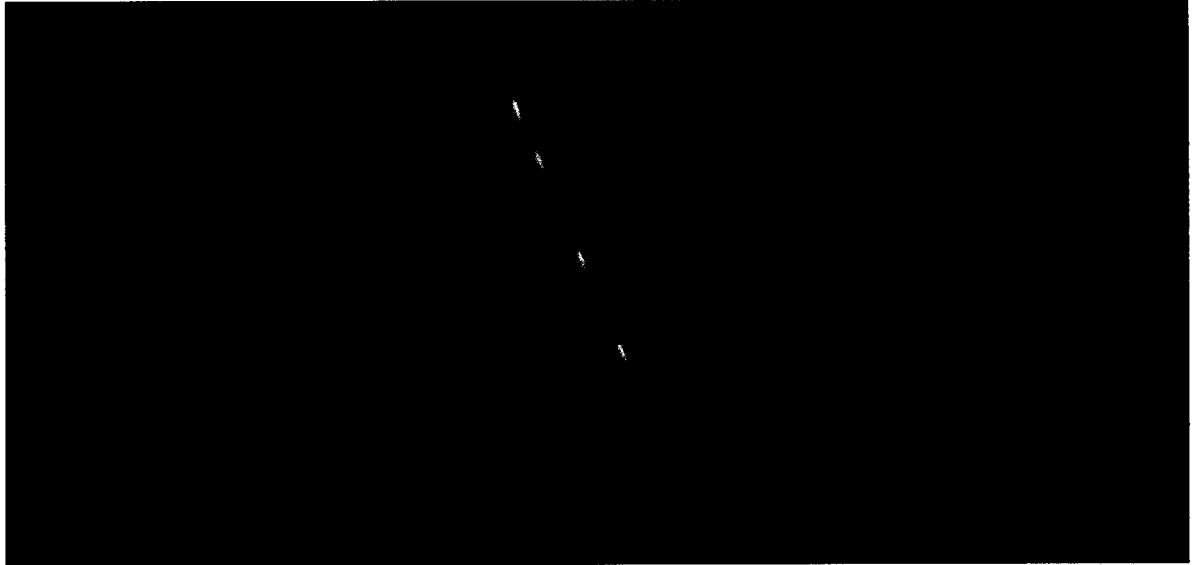
Figure 5.18: Flex body simulation

The Figure below shows the deflected shape of the flexible shaft with the first natural frequency. The flexible shaft has four different natural frequencies, which are:

54.4358886731 Hz

54.4470904505 Hz

136.600057531 Hz

136.796012567 Hz
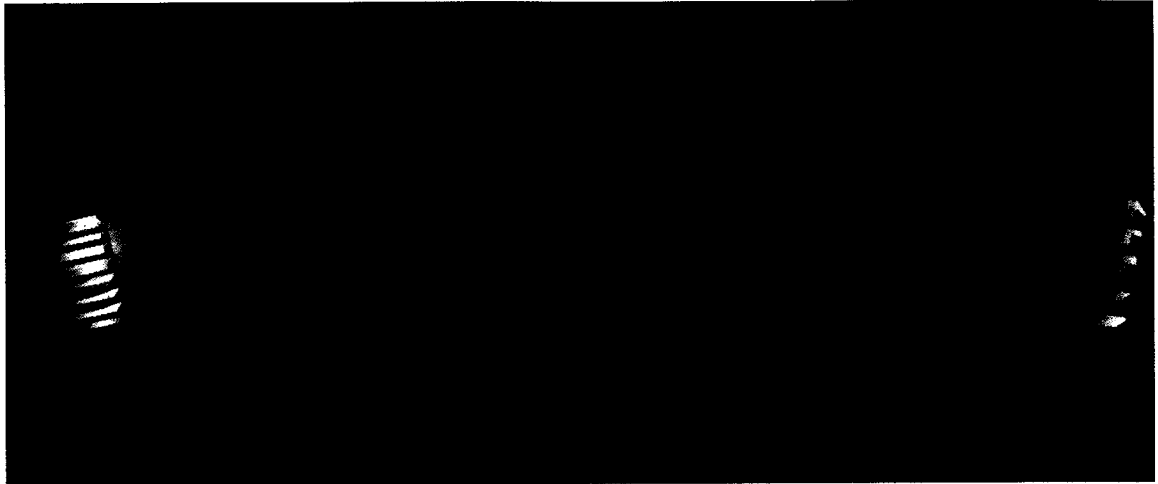
Figure 5.19: The shaft mode shapes

Note in Figure 5.20 below, the intake pistons show the highest deflection with a stress concentration, we can see red spots at the tip of the piston where it is connected to the slipper; this region should be investigated more closely to avoid failure.

Figure 5.20: The flex piston deformation

We can notice that the hot spot where the stress is the highest is in the shaft-barrel interface on the splines. The value of the Von-Mises stress is about $326.263 N/mm^2$. These results are different than the static analysis done by MSC.NASTRAN®. One thing to be mentioned is that the ends of the shaft are not subjected to a torque but only to a rotational motion. Therefore, the finding that can be helpful to the designers is the stress distribution and hot spots due to the dynamic motion and the deformation of the shaft. These have a maximum that occurs on the splines.

Von Mises Stress (MPa) Max at Node 35668 Time 0.001

327.0073
294.3066
261.6059
228.9053
196.2046
163.5039
130.8032
98.1025
65.4018
32.7011
4.4314E

Figure 5.21: The Von-Mises stress distribution

Figure 5.22: The shaft deformation from ADAMS/DURABILITY

The next step is to introduce the pistons as flexible parts and run the simulation again in order to get a model that is as much as possible close to the real world and investigate the strength of the parts and the interaction between the moving parts. The critical parts are the only ones that were made flexible based on the FEA analysis (Chapter 4).

All the pistons and the shaft are flexible parts and here below are the list of the highest values of the Von Mises stresses on all nine pistons and the shaft.

Piston: 243.526 N/mm^2

Piston_1: 243.353N/mm^2

Piston_2: 232.386N/mm^2

Piston_3: 235.922N/mm^2

Piston_4: 214.567N/mm^2

Piston_5: 181.723N/mm^2

Piston_6: 188.393N/mm^2

Piston_7: 209.246N/mm^2

Piston_8: 220.276N/mm^2

Shaft: 326.263N/mm^2

We notice that the highest stress occurs on the first piston and is around 243.5N/mm^2, while the shaft undergoes a stress of 326.3N/mm^2.

Here are the hot spots on the most critical parts, the piston and the shaft:

Table 5.4: VON MISES stresses for FLEX_SHAFT

VON MISES Hot Spots for FLEX_SHAFT						
Model= .FULL_ASSEMBLY		Analysis= Last_Run		Date= 2004-04-14 16:13:44		
Top 6 Hot Spots			Radius= 0.0 mm			
Hot Spot	Stress	Node	Time	Location wrt LPRF (mm)		
#	(newton/mm**2)	id	(sec)	X	Y	Z
1	326.263	35668	0.001	16.334	-12.9157	-58.5
2	321.089	34590	0.001	-18.9503	8.63138	-58.5
3	319.675	33372	0.096	-12.7685	16.4493	-58.5
4	318.202	37659	0.001	18.9503	-8.63137	-58.5
5	316.494	39916	0.093	-3.66152	-20.499	-58.5
6	314.807	38074	0.093	3.66152	20.499	-58.5

Table 5.5: VON MISES stresses for FLEX_PISTON

VON MISES Hot Spots for FLEX_BODY						
Model= .FULL_ASSEMBLY		**Analysis= Last_Run**	**Date= 2004-04-14 16:13:44**			
Top 6 Hot Spots			**Radius= 0.0 mm**			
Hot Spot	**Stress**	**Node**	**Time**	**Location wrt LPRF (mm)**		
#	**(newton/mm**2)**	**id**	**(sec)**	**X**	**Y**	**Z**
1	243.526	34909	0.003	1.61573e-006	-4.13811	6.38954
2	192.447	580	0.071	3.51523	-5.28934	73.773
3	164.178	6531	0.055	1.3284	3.54068	6.60674
4	160.944	10257	0.003	-0.3243	-5.55511	7.29697
5	154.01	6190	0.053	-1.84481	6.78782	-2.91284
6	153.4	518	0.006	3.89081e-007	7.59255	0.557585

For the Von Mises strains on all the flexible parts, we have:

Piston: 0.00291393mm/mm

Piston_1: 0.00291291mm/mm

Piston_2: 0.00278735mm/mm

Piston_3: 0.00285648mm/mm

Piston_4: 0.00262969mm/mm

Piston_5: 0.00216365mm/mm

Piston_6: 0.00221174mm/mm

Piston_7: 0.00249224mm/mm

Piston_8: 0.00262969mm/mm

Shaft: 0.00228025mm/mm

Here are the hot spots for the Von Mises strains on the most critical parts, the piston and the shaft:

Table 5.6: VON MISES strains for FLEX_SHAFT

VON MISES Hot Spots for FLEX_SHAFT						
Model= .FULL_ASSEMBLY		Analysis= Last_Run		Date= 2004-04-14 16:13:44		
Top 6 Hot Spots				Radius= 0.0 mm		
Hot Spot	Strain	Node	Time	Location wrt LPRF (mm)		
#	(mm/mm)	id	(sec)	X	Y	Z
1	0.00228025	35668	0.001	16.334	-12.9157	-58.5
2	0.00226472	36054	0.001	-16.334	12.9157	-58.5
3	0.00226322	34590	0.001	-18.9503	8.63138	-58.5
4	0.00225235	894	0.001	-14.2329	14.472	-106.354
5	0.00223931	35068	0.08	-10.8527	-17.7717	-58.5
6	0.00223881	34652	0.001	-14.7903	14.6581	-58.5

Table 5.7: VON MISES strains for FLEX_PISTON

VON MISES Hot Spots for FLEX_BODY						
Model= .FULL_ASSEMBLY		Analysis= Last_Run		Date= 2004-04-14 16:13:44		
Top 6 Hot Spots				Radius= 0.0 mm		
Hot Spot	Strain	Node	Time	Location wrt LPRF (mm)		
#	(mm/mm)	id	(sec)	X	Y	Z
1	0.00291393	34909	0.003	1.61573e-006	-4.13811	6.38954
2	0.0022571	580	0.045	3.51523	-5.28934	73.773
3	0.00195635	34907	0.003	2.15642e-006	-5.5229	5.24016
4	0.00193456	10257	0.003	-0.3243	-5.55511	7.29697
5	0.00193314	6531	0.055	1.3284	3.54068	6.60674
6	0.00183942	520	0.006	3.72577e-007	7.27047	2.25619

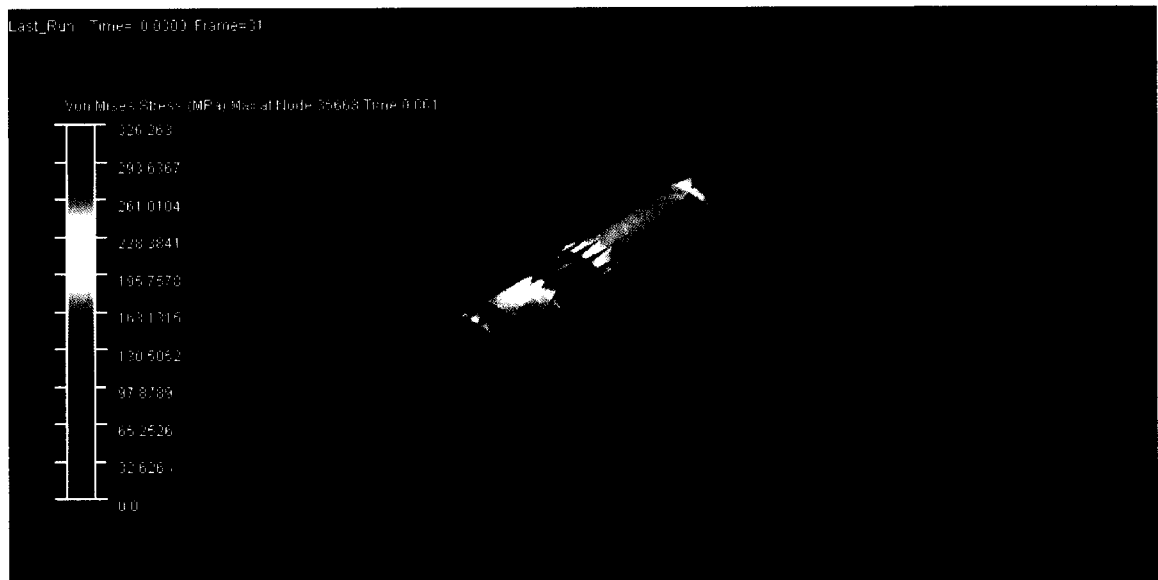Figure 5.23: Von Mises stresses on the shaft and pistons

Figure 5.24: Von Mises stresses on the most critical parts: shaft and piston

Notice that we have run the simulation for much finer steps in order to get more accurate results and we found that the Von Mises stresses had minimal changes; from 243.526 to 244.342, and from 326.263 to 327.007, which is less than 0.5% change (0.1 and 1000, 10000 steps).

5.7 Conclusion:

The important results that we can get from flex body simulation were investigated carefully and validated using some theoretical calculations. The results that we got are shown in the previous Figures above, with a comparison between the rigid and flex body simulation. The objective of the flex body simulation is to determine the different forces and reactions on the joints and parts upon dynamic motion of the pump, i.e., to try to model as close as possible the real world behavior of the pump and investigate the weaknesses and the parts that are most likely subjected to high stress concentration, which may lead to failure after a number of cycles.

Another objective of the flex simulation, mentioned earlier is the vibration study of the parts while they are assembled together and in dynamic motion. The different mode shapes and the different frequencies of the flexible parts give this. It allows the calculation of more accurate loads in systems with dependent structure components.

Also a third objective, which may be done by using the full package of ADAMS, i.e., using ADAMS/DURABILITY, allows us to investigate the stress distribution and identifying the hot spots upon dynamic motion of the full assembly.

6   CONCLUSION

Conclusions and Recommendations

6.1 Conclusions and Recommendations (FEA):

Although some of the components experience very high stresses (Ref.9), these stresses are below the maximum yield strength specified by Parker engineers. The shaft, piston, and swashplate exhibit stresses many times that of the barrel. Therefore while the other components must be made of a very high strength material, the barrel could be made of mild steel. The stresses on the piston are very high and would require a material with very high yield strength. The stresses could be lowered if the area was increases on the walls of the piston.

Overall the components were modeled very conservatively. The loads on each part were at least twice the actual loads the pump will ever see operating at the maximum pumping capacity at a given swash plate angle of 23°.

6.2 Conclusions and Recommendations (ADAMS):

The Flex body simulation of the full assembly of the pump was successfully modeled for the maximum output pressure of 42MPa. The main parameters such as the forces on the joints, the contact forces the kinetic energy, the mode shapes and the deflection of different component were investigated. Some of the results were validated by hand calculation and errors were found to be minimal (less than 5%). Connectivity between the Finite Element Analysis and the ADAMS dynamic simulation was successful by providing Modal neutral-files (mnf) to ADAMS in order to insure correct implementation of the Flex body simulation. Further study and analysis could be made concerning the Von-Mises stresses and the change in the stress distribution upon dynamic motion with the use of ADAMS/DURABILITY, but the mnf files provided must contain the history of the stress distribution.

The importance of the flex body is that the flex parts have different mode shapes embedded in the part that can give us an idea of how the part will vibrate upon dynamic motion. So this rise a difference from the Finite Element Analysis made on NASTRAN/PATRAN, the applied forces here are being dynamic, while the applied forces used in FEA analysis are static. Therefore, one can investigate the different mode shapes of the parts while is in dynamic motion. Moreover, the flex body simulation provides us with the study of the stress distribution and variation with the dynamic motion of the pump and the interaction between the different parts together as one assembly. This is different from the static analysis performed with Finite Element Analysis. The analysis of a complete assembly in

85

dynamic mode gives a better idea and knowledge about the stresses and will be helpful in the design process in order to predict failure of the parts.

Therefore, the shaft is the critical component compared to the pistons because it is found that the center of mass changes position, or in other words deform by a magnitude of 0.099mm, while the piston deforms by a magnitude of 0.02mm. Both results are not high and may not cause failure of the system but the shaft may be reviewed in order to lower the deflection.

References:

1. "Modeling and Virtual Prototyping of Parker- Hannifin's Piston Pumps," a grant proposal submitted by YSU to Parker-Hannifin, June 10, 2003.

2. Hydrostatic Pumps and Motors, Ivantsysn J., and Ivantnsynova M., Akademic Press, New Delhi, India, 2000.

3. "Torque on the Swashplate of an Axial Piston Pump," Zeiger, G. & Akers, A, *Transactions of ASME,* Vol. 107, September 1985.

4. http://www.cad.luth.se/help/swdocuments/adams/flex/flex.pdf

5. ADAMS/View 2003 Help

6. ADAMS/Flex 2003 Help

7. http://www.mscsoftware.com

8. R. R. Craig and M. C. C. Bampton. Coupling of substructures for dynamics analyses. AIAA Journal, 6(7): 1313-1319, 1968

9. Modeling and Virtual Prototyping of Parker- Hannifin's Piston Pumps, Report Phase II, March 2004.

10. Fluid Power Control with Applications, Fourth Edition, Prentice Hall